SYSTEM REQUIREMENTS FOR A DUAL POLARIZED SPACE TO EARTH COMMUNICATIONS LINK

by

Robert Edward Castle, Jr.

Thesis submitted to the Graduate Faculty of the
Virginia Polytechnic Institute and State University
in partial fulfillment of the requirements for the degree of
MASTER OF SCIENCE
in
Electrical Engineering

APPROVED:

C. W. Bostian, Chairman

H. L. Krauss

E. A. Manus

June, 1978

Blacksburg, Virginia

ACKNOWLEDGEMENTS

The author would like to express his sincere thanks to Dr. Charles W. Bostian for his advise, aid and encouragement during the research and preparation of this thesis. Special thanks are extended to Dr. W. L. Stutzman for his time and advise. Many of the results of this thesis were the result of late night discussions with to whom very special thanks are extended. The experimental data presented in this thesis are the result of work done by the Satellite Communications Group at VPI&SU and their combined aid is sincerely appreciated.

TABLE OF CONTENTS

LIST OF FIGURES

LIST OF TABLES

CHAPTER 1

INTRODUCTION

The demand for expanded satellite communications channels is causing system engineers to look to higher and higher frequencies and to methods for frequency reuse. In terms of capacity, the 20 and 30 GHz bands are extremely promising and their use is under consideration. The high antenna gains achievable at 20 and 30 GHz will allow frequency reuse through spatial diversity. Frequency reuse on orthogonal polarizations could double the available bandwidth and is being vigorously investigated. The main problems in designing 20 and 30 GHz satellite systems are the effects of rain. Rain severely attenuates signals at these high frequencies and also depolarizes them, resulting in crosstalk between orthogonal channels.

This thesis will examine system level constraints on dual polarized 20 and 30 GHz satellite links. The effects of crosstalk on channel performance, the effects of rain on the signal, and the requirements of dual polarized antennas will be evaluated in a form suitable for system calculations. These results will then be applied to a specific example, the Millimeter Wave Communications Experiment.

The impact of attenuation and rain induced crosstalk on system performance is the subject of Chapter 2. Crosstalk will be defined in terms of the *isolation* between the two channels of a dual polarized system. Isolation is defined as the ratio of the desired signal power to the interfering signal power present at the antenna

port. For perfect antennas and no depolarization the isolation is infinity. The world is going digital and digital modulation methods, chiefly PSK or QPSK, are planned for future satellite systems. In Chapter 2 QPSK will be assumed and the results stated for PSK and M-ary phase shift keying. An important concept derived in Chapter 2 is CNR degradation which expresses the effects of crosstalk as a degradation of the carrier to noise ratio.

With the effects of attenuation and crosstalk calculated, Chapter 3 considers how to determine the attenuation and depolarization caused by rain. Data on rain attenuation and depolarization are currently being measured at VPI&SU. Though very useful in testing theoretical models, in general, empirical data is too expensive and too limited in location to be used for system design. A suitable theoretical model is required which is adaptable to many locations and elevation angles. Rain modeling is reviewed and a new model is discussed which has compared well with measured data. The results of this model are combined with a rain rate model, and the CNR degradation derived in Chapter 2, so as to predict *effective* attenuation statistics.

Possible problems with antenna effects are taken up in Chapter 4. These include polarization purity, polarization tracking of elliptically polarized waves, and antenna pointing accuracy.

The first true test of a dual polarized 20/30 GHz digital satellite link will come with the Millimeter Wave Communications Experiment (MWCE) [1] which is a proposed Spacelab experiment.

Spacelab is a manned orbital laboratory which is carried aloft by the Space Shuttle. The Spacelab remains in the shuttle payload bay and provides a stable platform for experiments in low earth orbit.

The MWCE will operate in several modes: CW beacon, high data rate (50 Mbps) single and dual polarized, uplink only, downlink only, and a transponder mode where the uplink is transmitted back to the ground station by the spacecraft. From the low orbit shuttle all elevation angles can be investigated and for very low elevation angles the MWCE will furnish the first experimental data at 20 and 30 GHz.

VPI&SU is one of the proposed ground stations for the MWCE and this thesis is geared toward that experiment. Chapter 5 examines in detail the required EIRP and G/T of the ground station, and predicts link outage times for the VPI&SU location.

Though the MWCE is the chosen example, the methods outlined in this thesis are applicable to *any* digital satellite communications system, single or dual polarized, low orbit, synchronous orbit, or "beyond."

CHAPTER 2

SYSTEM REQUIREMENTS IMPOSED BY MODULATION

The modulation scheme selected for the MWCE and planned for other systems is quad phase shift keying (QPSK). This system uses bandwidth more efficiently than Bi phase shift keying (BPSK) and like most digital modulation techniques is fairly tolerant of noise and interference. Exactly how tolerant is the subject of this chapter. The probability of symbol error will be derived in terms of the carrier to noise ratio and the carrier to interference ratio. An upper bound to the probability of symbol error will be developed which yields good results and is simpler to calculate than the exact solution. Finally, a simple method to apprxoimate accurately the carrier to noise ratio degradation caused by interference will be developed. This degradation is easily included in system power budgets or extended to M-ary phase shift keyed systems.

2.1 Probability of Symbol Error for a QPSK System Corrupted By Coherent Interference and Gaussian White Noise

A QPSK signal is best described by a phasor diagram as illustrated in Figure 2.1-1. The desired signal has an amplitude $\sqrt{2C}$, where C is the energy per symbol, and is assumed to have a phase angle as shown in the figure. An interfering or unwanted signal with amplitude $\sqrt{2I}$ and phase angle λ is added to the original signal by crosstalk. Narrowband Gaussian white noise can be represented by

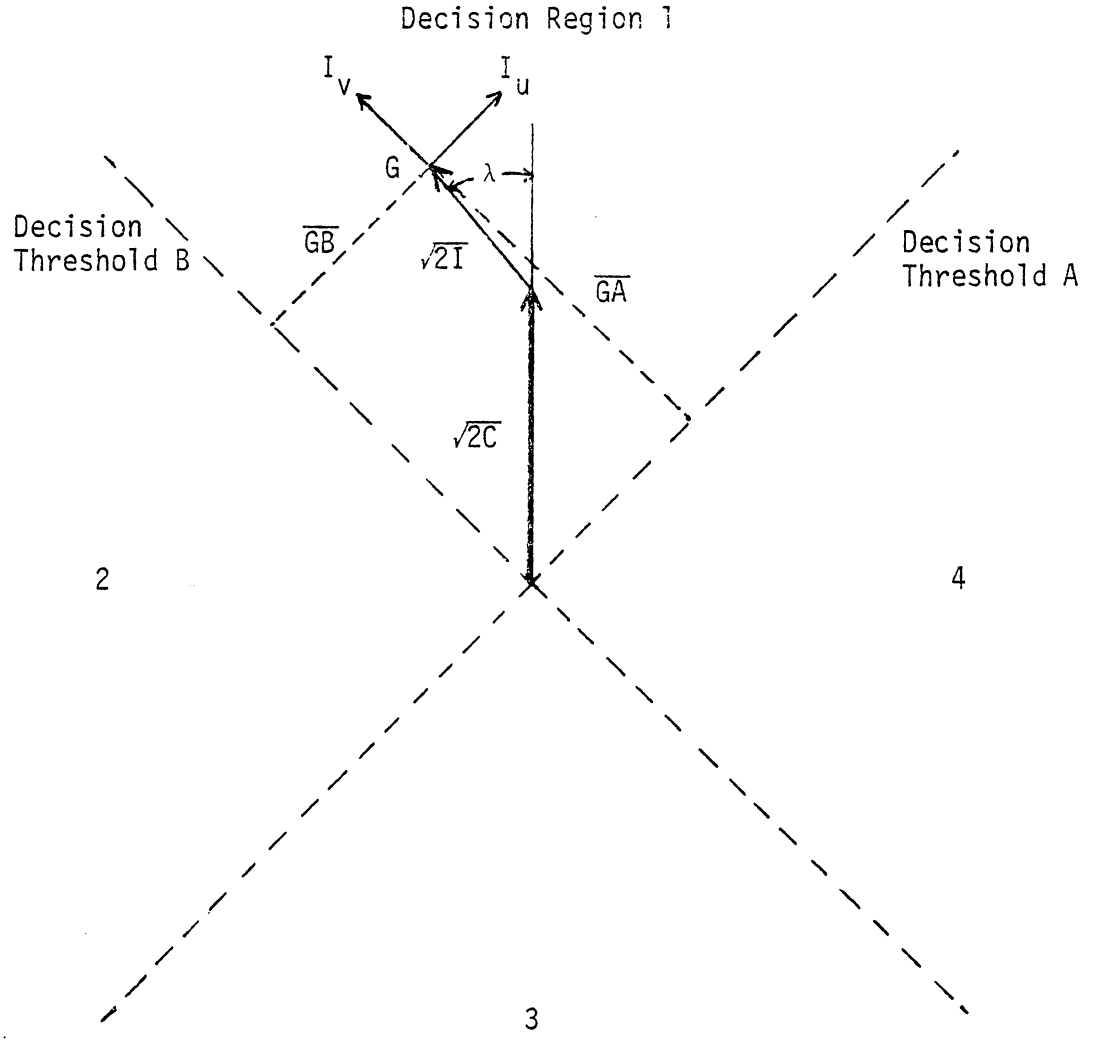

Figure 2.1-1. Phasor diagram of a QPSK signal and interference.

two orthogonal vectors whose amplitudes are Gaussian random variables [2]. These vectors are shown in Figure 2.1-1 with amplitudes I_u and I_v which have zero means and are statistically independent with variances (powers) of σ^2. The actual received signal is the vector sum of the desired signal C, the interfering signal I, and the noise I_u and I_v. As long as the tip of the resultant vector lies in the same decision region as the desired signal, no error is made.

The probability of error is equivalent to the probability of the noise being larger than the distance from a decision threshold to the tip of the vector sum of C and I. The distance from the tip of the vector sum (point G) to the decision threshold A is found from geometry to be

$$\overline{GA} = \sqrt{2C}\,\sin(\tfrac{\pi}{4}) + \sqrt{2I}\,\sin(\tfrac{\pi}{4} + \lambda) \qquad (2.1\text{-}2)$$

where $\overline{GA}$ is the indicated distance. Similarly $\overline{GB}$ is found to be

$$\overline{GB} = \sqrt{2C}\,\sin(\tfrac{\pi}{4}) + \sqrt{2I}\,\cos(\tfrac{\pi}{4} + \lambda) \quad . \qquad (2.1\text{-}2)$$

Define P_u to be the probability that $-I_u \geq \overline{GB}$ and P_v to be the probability that $-I_v \geq \overline{GA}$. Since I_u and I_v are Gaussian variables it is easily shown that

$$P_u = \frac{1}{2}\,\mathrm{erfc}\left(\frac{\overline{GB}}{\sqrt{2}\,\sigma}\right) \qquad (2.1\text{-}3)$$

$$P_v = \frac{1}{2}\,\mathrm{erfc}\left(\frac{\overline{GA}}{\sqrt{2}\,\sigma}\right) \qquad (2.1\text{-}4)$$

where

$$\text{erfc}(x) = \sqrt{\frac{2}{\pi}} \int_x^\infty e^{-u^2}\, du \quad .$$

P_u is the probability that the resultant vector (signal + interference + noise) lies in decision regions 2 or 3 and P_v is the probability that the resultant lies in regions 3 or 4. Therefore, the probability of symbol error, P_e, is

$$P_e = P_u + P_v - P_u P_v \quad .$$

It should be noted that symbol error is not the same as bit error for QPSK since one symbol consists of two bits. The bit error probability (BEP) is P_u or P_v depending on the bit in question. Usually BEP $\simeq \frac{1}{2} P_e$.

It is convenient to express P_e in terms of the carrier to noise ratio (CNR) and the carrier to interference ratio (CIR) since these are the important quantities to systems designers. Define

$$\rho = \sqrt{\frac{C}{\sigma^2}} \qquad \text{and} \qquad F = \sqrt{\frac{I}{C}}$$

where ρ is the square root of the energy per symbol divided by the noise spectral density and F is the square root of the interference to carrier ratio. The energy per symbol divided by the noise spectral density is equivalent to the carrier to noise ratio in the symbol rate bandwidth. Mathematically

$$\rho = 10^{\frac{CNR}{20}} \qquad \text{and} \qquad F = 10^{-\frac{CIR}{20}}$$

where CNR is the carrier to noise ratio in the symbol rate bandwidth expressed in dB and CIR is the carrier to interference ratio expressed in dB. Substituting ρ and F into 2.1-1 and 2.1-2 and rearranging yields

$$\frac{\overline{GA}}{\sqrt{2}\,\sigma} = \frac{\rho}{\sqrt{2}} + \rho\, F \sin(\frac{\pi}{4} + \lambda)$$

$$\frac{\overline{GB}}{\sqrt{2}\,\sigma} = \frac{\rho}{\sqrt{2}} + \rho\, F \cos(\frac{\pi}{4} + \lambda) \quad .$$

For a given ρ and F, P_e is dependent on λ and may be written as

$$\begin{aligned} P_{ec} = {} & \frac{1}{2}\,\mathrm{erfc}(\frac{\rho}{\sqrt{2}} + \rho\, F \cos(\frac{\pi}{4} + \lambda)) \\ & + \frac{1}{2}\,\mathrm{erfc}(\frac{\rho}{\sqrt{2}} + \rho\, F \sin(\frac{\pi}{4} + \lambda)) \\ & - \frac{1}{2}\,\mathrm{erfc}(\frac{\rho}{\sqrt{2}} + \rho\, F \sin(\frac{\pi}{4} + \lambda)) \\ & \times \frac{1}{2}\,\mathrm{erfc}(\frac{\rho}{\sqrt{2}} + \rho\, F \cos(\frac{\pi}{4} + \lambda)) \end{aligned} \qquad (2.1\text{-}5)$$

where P_{ec} is the probability of error with the interfering signal unmodulated. If the interferer is also QPSK modulated and has coincident symbol timing

$$\lambda = \theta + m(\frac{\pi}{2})$$

where m = 0,1,2,3 with equal probability and θ represents the phase of the interferer relative to the desired carrier. The P_e conditioned on θ may then be written as

$$P_e(\theta) = \frac{1}{4} \sum_{m=0}^{3} P_{ec}(\theta + m \frac{\pi}{2}) \quad . \tag{2.1-6}$$

From Figure 2.1-2 it can be seen that the distances $\overline{GA}$ and $\overline{GB}$ are minimized and therefore P_e is maximized for $\theta = 45°$. $\overline{GA}$ and $\overline{GB}$ are maximized and P_e minimized for $\theta = 0°$. Thus, $\theta = 45°$ is the worst case condition.

If the interfering signal is not coherently related to the desired signal, λ is assumed to be uniformly distributed between θ and 2π. The probability of error may then be approximated as

$$P_{eu} \simeq \frac{1}{N} \sum_{m=1}^{N} P_{ec}(m \frac{2\pi}{N}) \quad . \tag{2.1-7}$$

The exact solution of the probability of error with λ assumed to be uniformly distributed has been calculated by Prabhu [3] and Rosenbaum [4]. Curves plotted from equation 2.1-7 with N = 100 agree extremely well with the exact solution. Juroshek [5] has shown that 2.1-7 agrees very well with the exact solution for values of N as low as 20.

P_e as calculated from 2.1-6 for a carrier to interference ratio (CIR) of 10 dB and a relative phase shift (θ) of 0 and 45° is plotted in Figure 2.1-3. P_{eu} as calculated from 2.1-7 with N = 100 is plotted in Figure 2.1-3 for comparison. If there is no interference, F = 0 and 2.1-5 becomes

$$P_e(\text{no interference}) = \operatorname{erfc}(\frac{\rho}{\sqrt{2}}) - \frac{1}{4} \operatorname{erfc}^2 (\frac{\rho}{\sqrt{2}}) \quad . \tag{2.1-8}$$

This is a well known result and is also plotted in Figure 2.1-3.

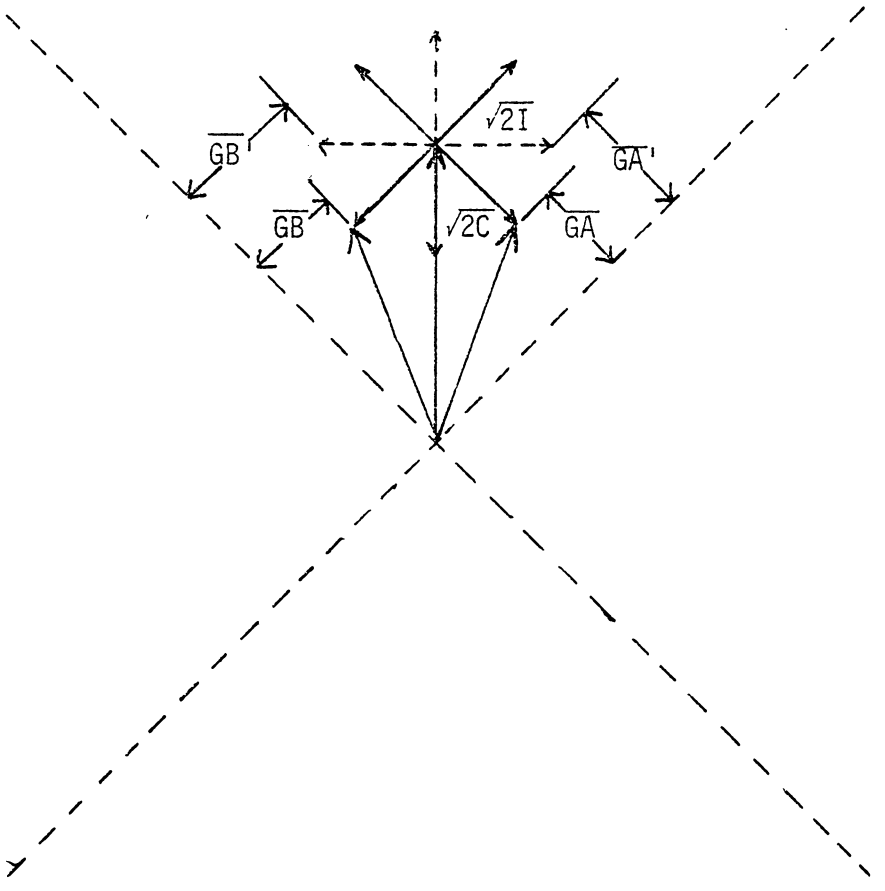

Figure 2.1-2. QPSK signal with interference.

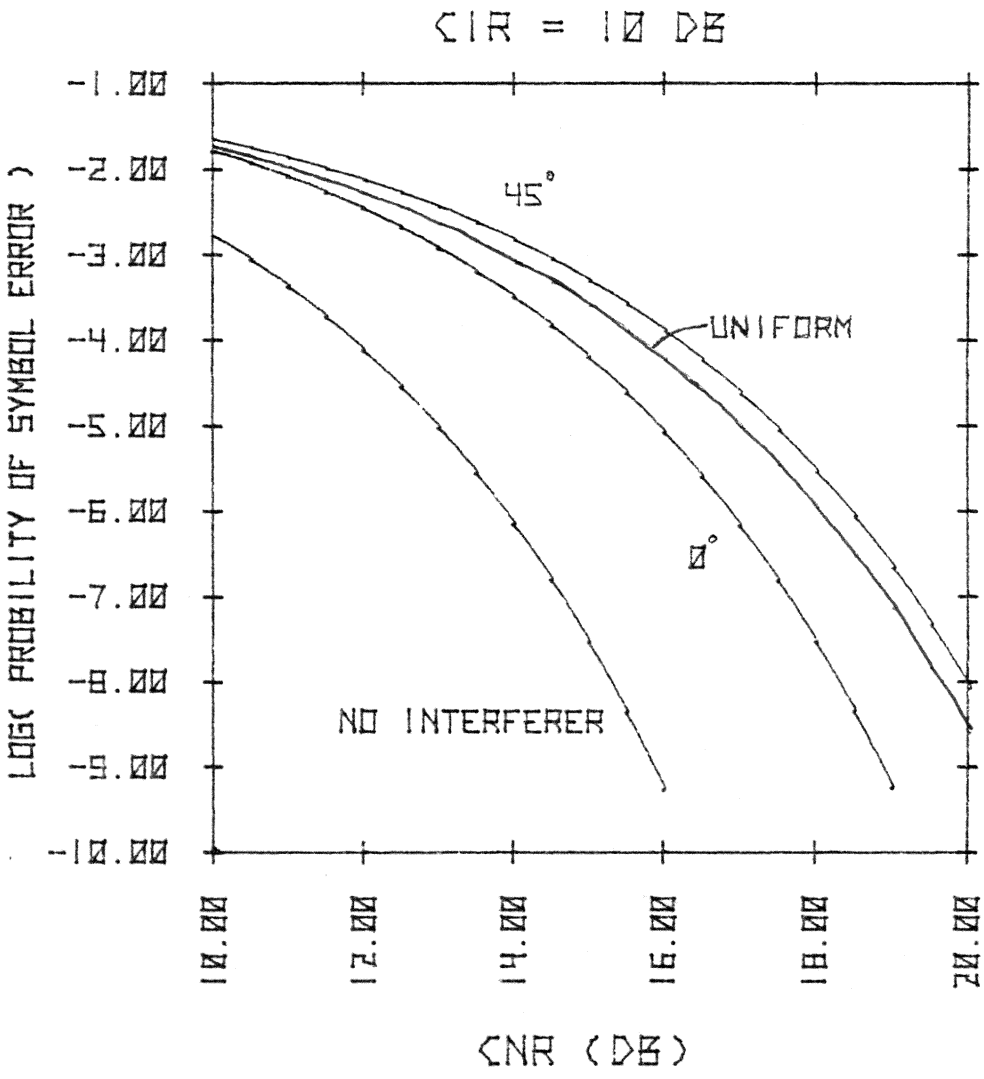

Figure 2.1-3. QPSK Probability of symbol error vs CNR.

The worst case P_e corresponding to $\theta = 45°$ is plotted in Figure 2.1-4 for several values of CIR. The probability of error for CIR = 30 dB is very close to the probability of error for no interference, so for all practical purposes a CIR greater than 30 dB has no effect on P_e.

The probability of error of a Bi phase shift keying system (BPSK) can be shown to be

$$P_{e\ BPSK}(\theta) = \frac{1}{2} \sum_{m=1}^{2} P_e(\theta + m\pi) \qquad (2.1\text{-}9)$$

where

$$P_e(\lambda) = \frac{1}{2} \operatorname{erfc}(\rho + \rho F \cos(\lambda)) \qquad (2.1\text{-}10)$$

and $\theta = 90°$ is the worst case.

2.2 Upper Bound of Probability of Error

Equation 2.1-6 is an exact expression for the probability of error but is somewhat cumbersome to evaluate. A simpler expression will be determined which sets an upper bound on P_e. Referring to Figure 2.1-1 it is easily seen that $\overline{GB}$ is minimum for $\lambda = 135°$. Therefore $P_{ec}(135°)$ is an upper limit on P_e.

$$P_{ec}(135°) = P_{emax} = \frac{1}{2} \operatorname{erfc}\left(\frac{\rho}{\sqrt{2}} - \rho F\right) + \frac{1}{2} \operatorname{erfc}\left(\frac{\rho}{\sqrt{2}}\right) - \frac{1}{4} \operatorname{erfc}\left(\frac{\rho}{\sqrt{2}} - \rho F\right) \operatorname{erfc}\left(\frac{\rho}{\sqrt{2}}\right) \qquad (2.2\text{-}1)$$

$\operatorname{erfc}(x) \geq 0$ therefore

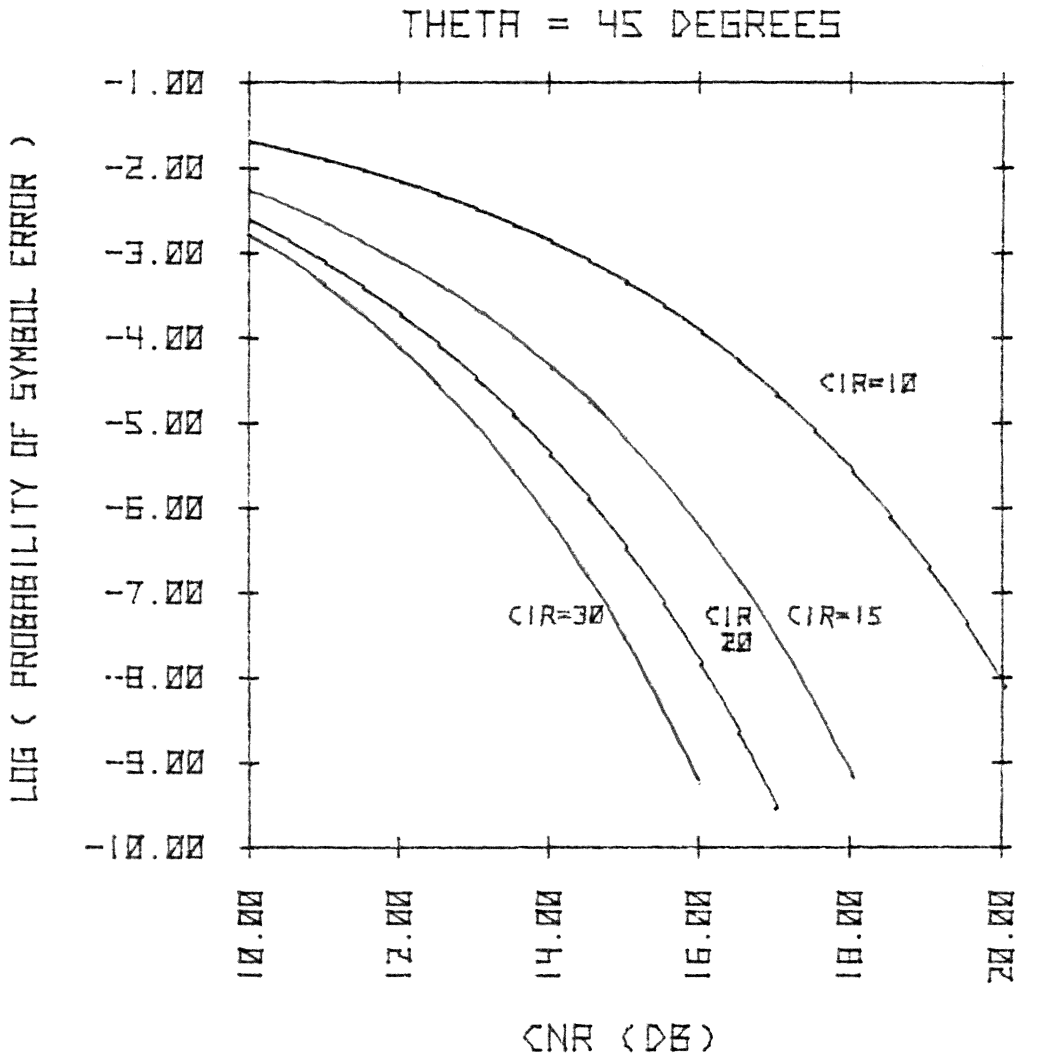

Figure 2.1-4. QPSK Probability of symbol error vs CNR for various CIR values.

$$P_{emax} \leq \frac{1}{2}\,\mathrm{erfc}\left(\frac{\rho}{\sqrt{2}} - \rho F\right) + \frac{1}{2}\,\mathrm{erfc}\left(\frac{\rho}{\sqrt{2}}\right)$$

$$\mathrm{erfc}\left(\frac{\rho}{\sqrt{2}} - \rho F\right) \geq \mathrm{erfc}\left(\frac{\rho}{\sqrt{2}}\right) \qquad \text{therefore}$$

$$P_{emax} \leq \mathrm{erfc}\left(\frac{\rho}{\sqrt{2}} - \rho F\right)$$

and $\mathrm{erfc}\left(\frac{\rho}{\sqrt{2}} - \rho F\right)$ is an upper bound on P_{emax}.

Define

$$P_{eub} = \mathrm{erfc}\left(\frac{\rho}{\sqrt{2}}(1 - \sqrt{2}\,F)\right) \quad . \tag{2.2-2}$$

P_{eub} and the worst case P_e are plotted in Figure 2.2-1 for a CIR of 15 dB. As can be seen from the figure P_{eub} is a fairly good approximation to the worst case P_e. The concept of this upper bound has been investigated by Juroshek [6] who has shown that the general expression for a M-ary phase shift keyed system is

$$P_{eub} = \mathrm{erfc}\left(\rho \sin\left(\frac{\pi}{M}\right)\left(1 - \frac{F}{\sin\left(\frac{\pi}{M}\right)}\right)\right) \quad . \tag{2.2-3}$$

2.3 CNR Degradation

In the preceeding sections expressions for the probability of error in terms of carrier to noise ratio and carrier to interference ratio have been developed. However, for system calculations it is much more convenient to express the effects of interference as a degradation of a required carrier to noise ratio. This CNR degradation is defined as the CNR required to achieve a specified P_e for a given CIR minus the CNR required to achieve the same P_e with

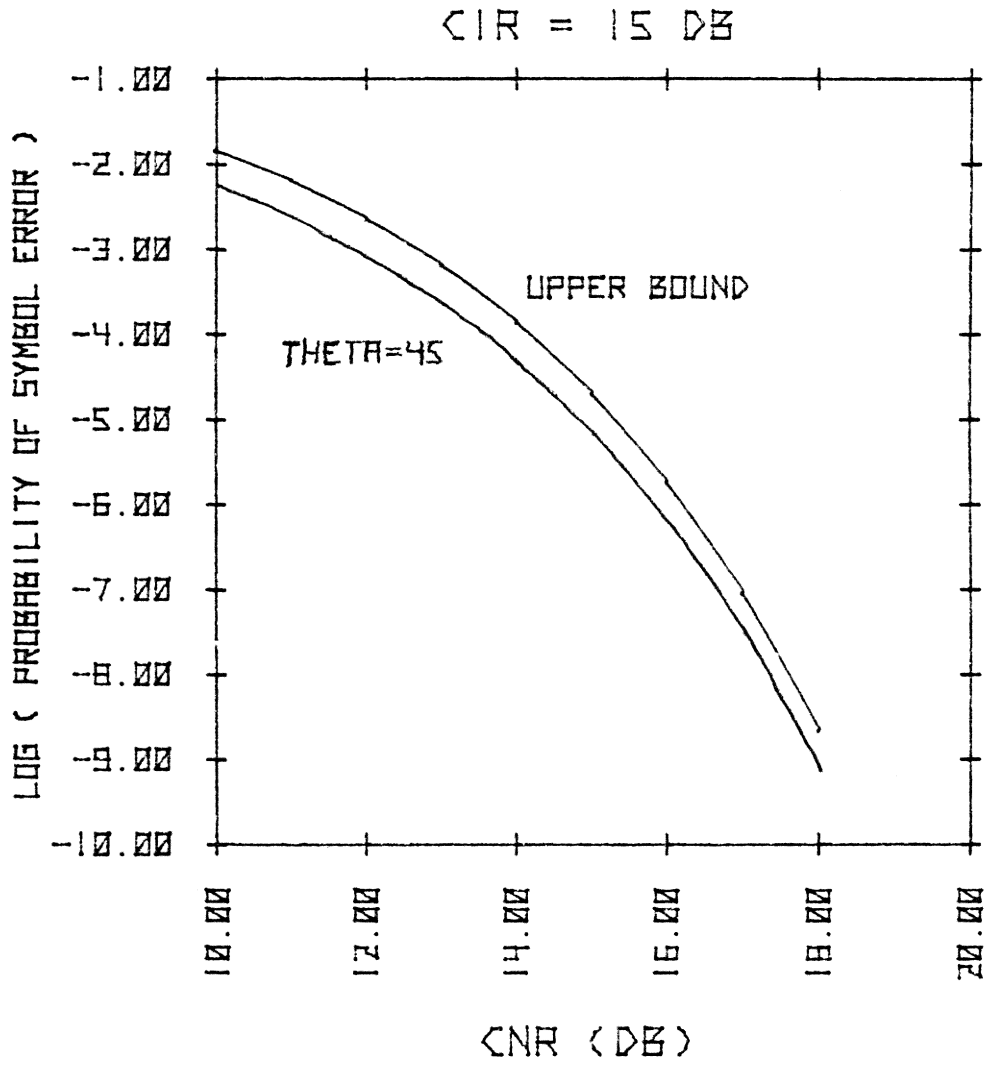

Figure 2.2-1. QPSK Probability of error; upper bound and exact.

no interference. Strictly speaking, CNR degradation is a function of the specified P_e as well as CIR. The CNR degradation for a $P_e = 10^{-5}$ with a relative phase shift θ of 0, 45°, and θ uniformly distributed is plotted in Figure 2.3-1. These curves are exact, but the calculations required to generate them (matching points generated by evaluation of equations 2.1-6 and 2.1-7) are extremely cumbersome.

Examination of equations 2.2-2 and 2.1-8 shows that P_{eub} is approximately equal to, but greater than P_e (no interference) with $\rho/\sqrt{2}$ multiplied by $1 - \sqrt{2}\,F$. Therefore $1 - \sqrt{2}\,F$ is an upper bound on the CNR degradation. Define

$$D_{ub} = 20 \log_{10}(1 - \sqrt{2}\,F) \text{ dB} \qquad (2.3\text{-}1)$$

where D_{ub} is the upper bound on CNR degradation expressed in dB and $F = 10^{-CIR/20}$. D_{ub} is plotted in Figure 2.3-2 with the exact CNR degradation for $P_e = 10^{-5}$ and $\theta = 45°$ (worst case) shown for comparison. As can be seen D_{ub} is a fairly good approximation to the exact degradation. Juroshek [5] has shown that the general form of D_{ub} for a M-ary PSK system is

$$D_{ub} = \left(1 - \frac{F}{\sin(\frac{\pi}{M})}\right) \quad . \qquad (2.3\text{-}2)$$

It should be noted that the upper bound CNR degradation is independent of the specified probability of error and the modulation of the interference (amplitude modulation excepted). D_{ub} is also applicable to bit error probability calculations for both symetric and nonsymetric channels. It is easily calculated and incorporated

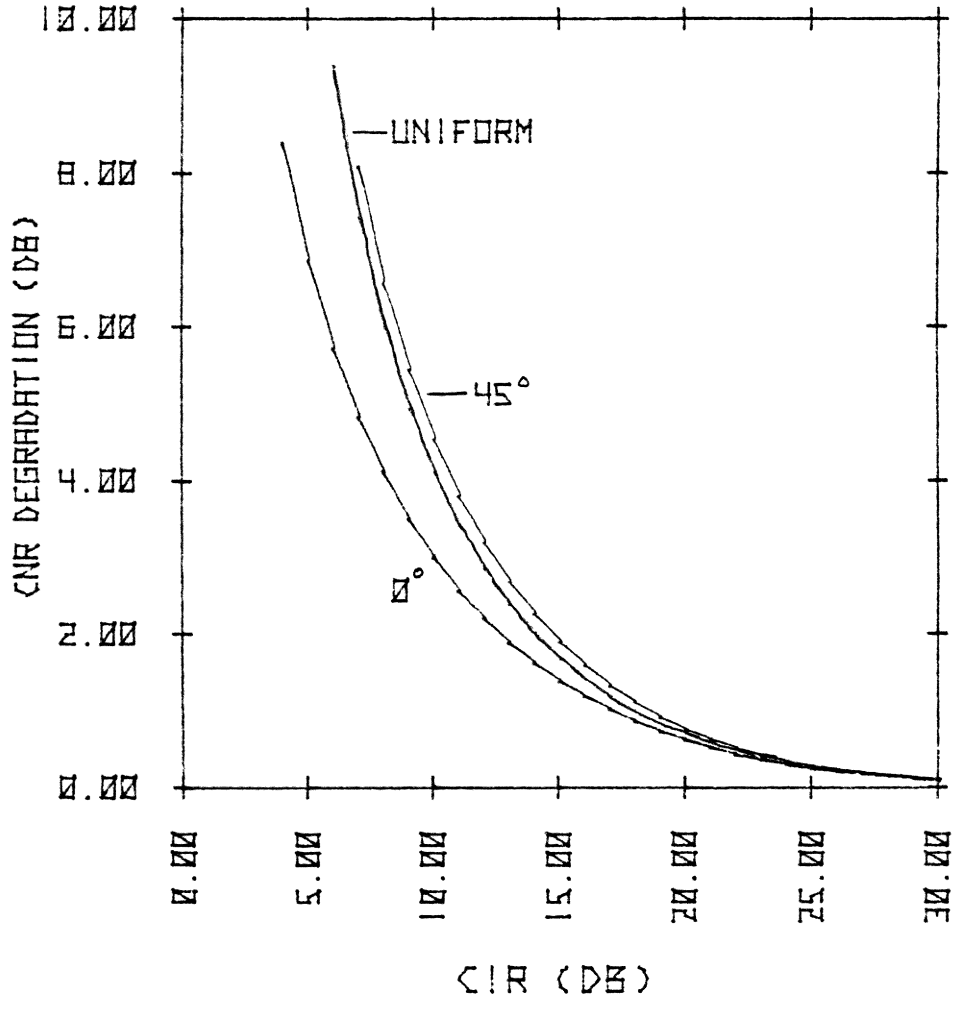

Figure 2.3-1. QPSK CNR Degradation with QPSK interference for 0, and 45° relative phase shift and for uniformly distributed phase shift.

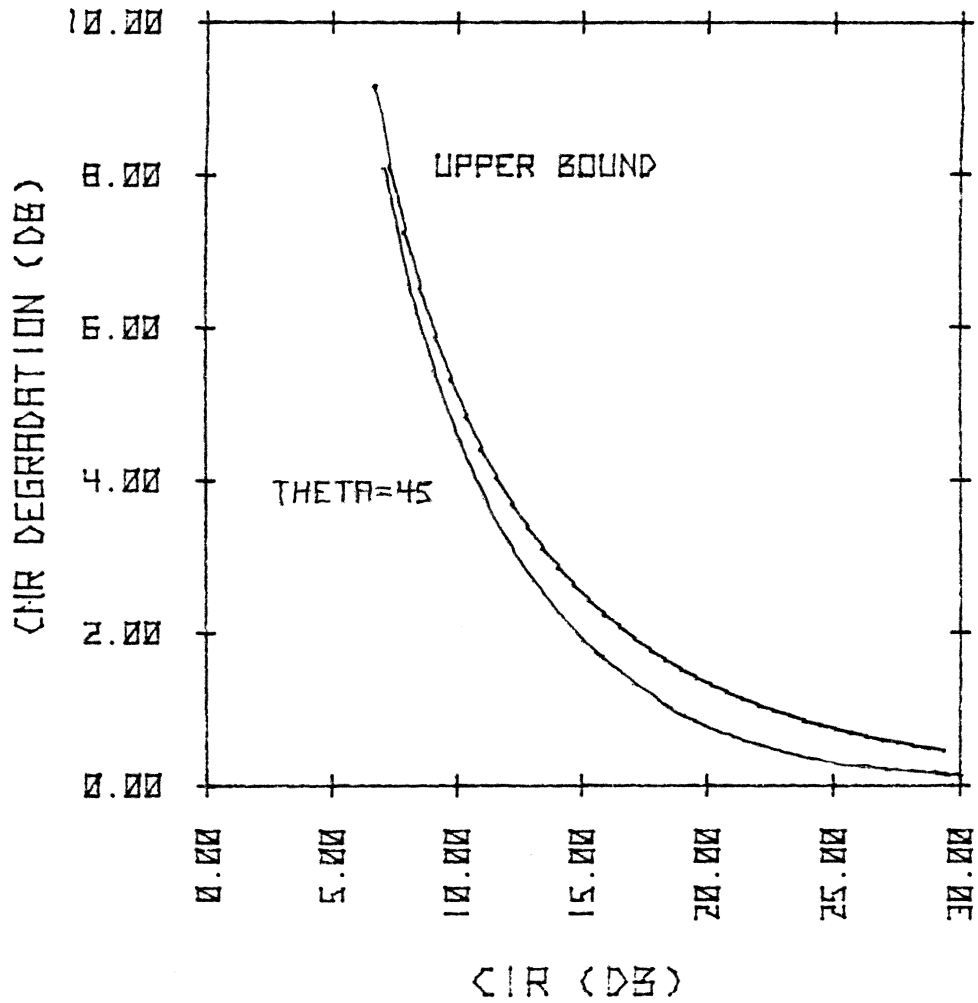

Figure 2.3-2. CNR Degradation: Exact for relative phase shift of 45° and upper bound.

into system power budgets.

CHAPTER 3

PROPAGATION MEDIUM EFFECTS ON COMMUNICATIONS

Propagation medium effects at 20 and 30 GHz consist almost entirely of molecular absorption by atmospheric gasses and scattering by hydrometeors. Ionispheric scintillation and Faraday rotation are troublesome at lower frequencies but negligible at 20 and 30 GHz. Molecular absorption is of course always present and essentially time independent. It is a function of the path length through the atmosphere which can be calculated from the ground station elevation angle. Once calculated, the loss due to absorption is included in the system power budget.

Loss due to scattering by hydrometeors is a more difficult problem because it varies widely with time and can be very severe. Of the hydrometeors present in the atmosphere rain is by far the most important. Rain both attenuates and depolarizes an incident electromagnetic wave. While theoretical modeling of the scattering by rain drops is well advanced, little is known about how the rain itself should be modeled. Modeling efforts to date will be described and the most successful model of the rain path will be used to predict attenuation and depolarization levels as a function of ground rain rate. These predictions will be compared to data measured at several locations.

It will be shown that attenuation will be quite severe for moderately high rain rates. Therefore the percent of time that a

given rain rate will be exceeded is an important design parameter. A statistical model for rain rate exceedence will be reviewed and results compared with measured data.

3.1 Effects of Molecular Absorption

Molecular absorption at 20 and 30 GHz is almost entirely due to oxygen and water vapor. The oxygen molecule possesses a permanent dipole moment and its interaction with the incident field causes a family of absorption lines in the vicinity of 60 GHz and a single line at 118.8 GHz. Water vapor is a polar molecule with an electric dipole moment. The interaction of the dipole moment with the incident field produces absorption lines at 22.5, 183.3 GHz and assorted higher frequencies.

Crane [7] and Hogg [8] have presented theoretical results that predict the one way zenith attenuation due to oxygen and water vapor. Oxygen absorption is dependant on atmospheric pressure and temperature but the dependance is minor. Water vapor absorption is additionally dependant on the humidity. Hogg and Crane's results indicate a typical value of one way attenuation of 0.3 dB at 20 GHz and 0.2 dB at 30 GHz for a U. S. Standard atmosphere. Crane notes that the calculated values may be optimistic by as much as a factor of 1.5. Therefore the values of 0.45 dB at 20 GHz and 0.33 dB at 30 GHz will be used as a worst case estimate. These values are for a zenith path. In general the attenuation A_a will be computed by the flat earth formula

$$A_a = A_z/\sin \alpha \qquad (3.1\text{-}1)$$

where A_z is the zenith attenuation and α is the elevation angle.

$$A_z = \begin{cases} 0.45 \text{ dB at } 30 \text{ GHz} \\ \\ 0.33 \text{ dB at } 30 \text{ GHz} \end{cases} .$$

3.2 Rain Effects

Rain attenuates and depolarizes electromagnetic waves. This problem was first considered by Oguchi [9] who calculated the scattered field due to a single oblate raindrop. Oguchi's published single drop scattering coefficients were later verified by Morrison and Cross [10] and Uzunoglu, Evans and Holt [11]. Using the theory of van de Hulst [12] Oguchi extended the single drop solution to an ensemble of identical, equioriented oblate raindrops.

Raindrops are not all the same size and Thomas [13] extended Oguchi's work by incorporating the Laws and Parsons [14] drop size distribution in the model. Watson [15] and Chu [16] further refined Thomas' model but their work required all drops to be oblate and equioriented and the rain rate to be uniform along the path.

At this point the capabilities of the theoretical models have exceeded the known rain characteristics. Meteorologists Jones [17] and Prupacher and Pitter [18] disagree on whether all drops are oblate or whether many of them are spherical or irregular. This point is important since spherical drops do not depolarize (see)

Figure 3.2-1). Wiley [19] has shown that as few as 40% of the drops can be assumed to be oblate with the rest assumed spherical and the theory still agree with data measured on a terrestrial path. Persinger [20] has found that assuming 60% of the drops are oblate agrees well with isolation data measured on a satellite path at 11, 19 and 28 GHz.

The work of Saunders [21] has indicated that drop canting angles have a Gaussian distribution. A Gaussian distribution of canting angles has been used in the models developed by Persinger and Uzunoglu et al. However there is no data from which the mean and standard deviation σ can be determined. Brussaard [22] has shown that the mean will be a function of the local wind gradient though it is probably close to zero. Existing data on the standard deviation σ of the canting angle are in conflict. As is illustrated in Figure 3.2-2 the choice of σ has a significant effect on the estimated isolation (in the figure the polarization is circular so the mean has little effect). Examination of Figures 3.2-1 and 3.2-2 show that many combinations of σ and the percent of oblate drops will yield the same curve thus complicating their determination from experimental data.

Though σ and the percent oblate are important to depolarization measurements they have little effect on the predicted attenuation. The usual method of predicting attenuation is expressed as

$$A(R) = A_s(R)L_e \qquad (3.2\text{-}1)$$

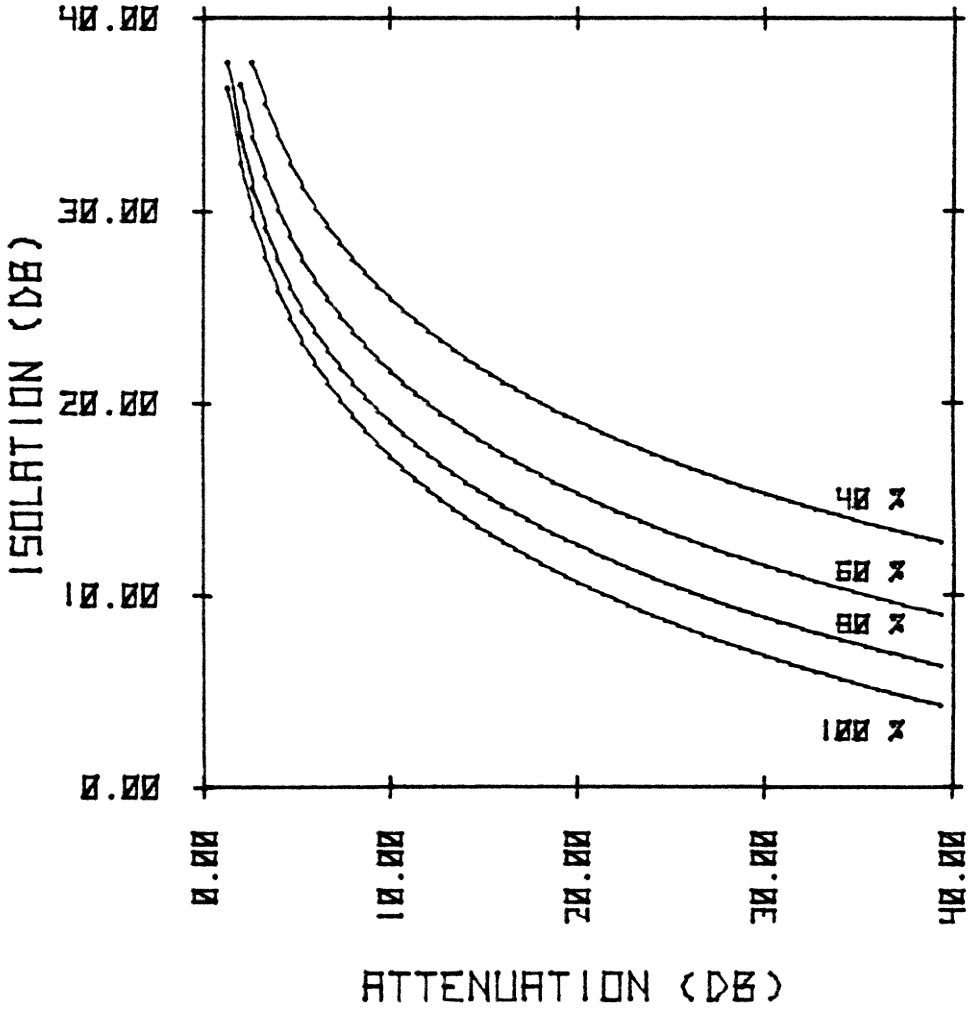

Figure 3.2-1. Isolation vs attenuation for 40, 60, 80 and 100% oblate raindrops. f = 20 GHz. Circular polarization. Path length 8.2 km.

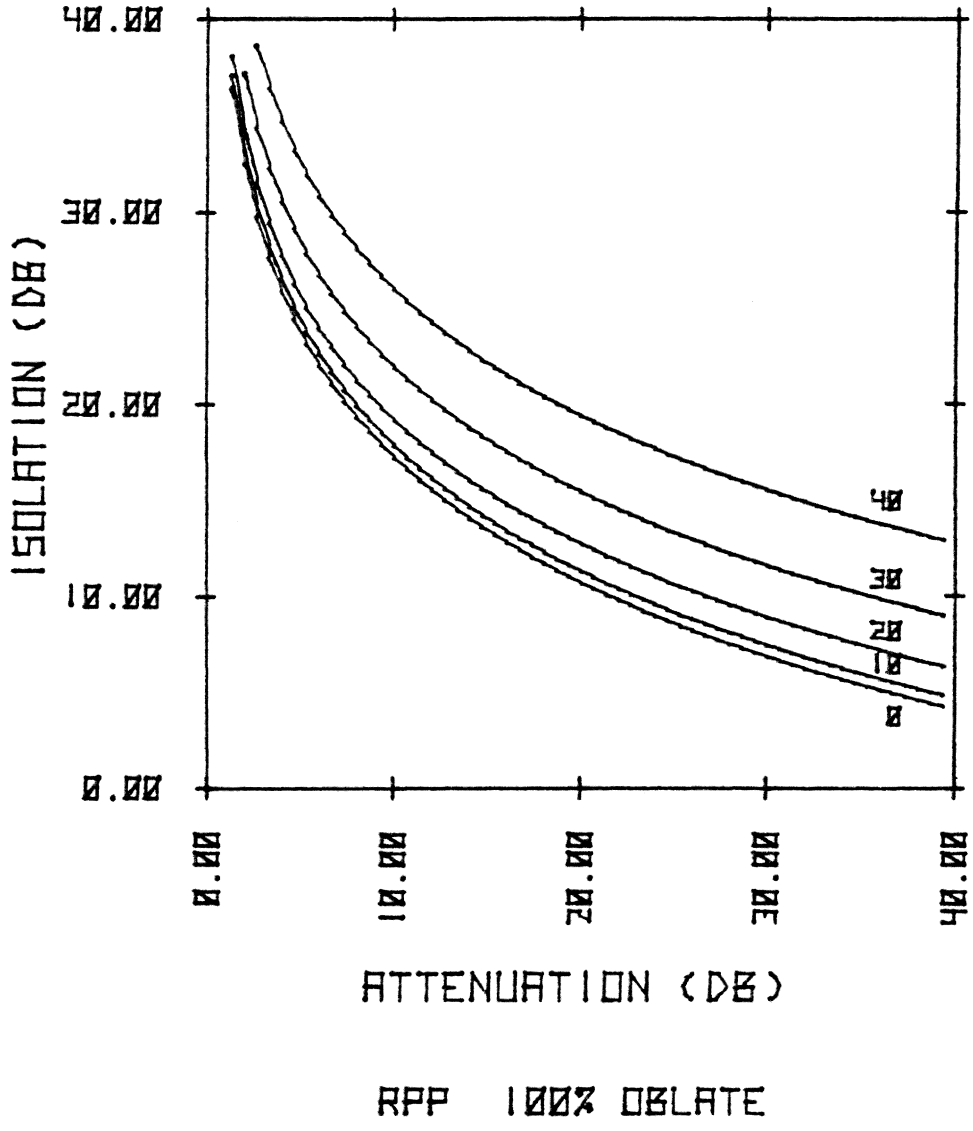

Figure 3.2-2. Isolation vs attenuation for canting angle standard deviations of 0, 10, 20, 30 and 40 degrees. f = 20 GHz. Circular polarization. Path length 8.2 km.

where A(R) is the path attenuation at rain rate R, A_s is the attenuation per km for a uniform rain rate R and L_e is the effective path length. This is a convenient method since A_s is available both in the form of curves and simple aR^b equations. This formulation works fairly well for terrestrial links where the path length is known. However, for a satellite path L_e is not known. It cannot be calculated from geometry because 3.2-1 assumes uniform rain rate on the path and this is *not* true. A light rain tends to be widespread while a heavy rain is more limited in extent. For 3.2-1 to be accurate L_e must be a function of the rain rate R.

Several experimenters [23], [24], [25], have measured L_e according to the equation

$$L_e(R) = \frac{A(T)}{A_s(R(T))} \qquad (3.2\text{-}2)$$

where A(T) is the measured attenuation exceeded for T percent of the time, R(T) is the rain rate exceeded T percent of the time and $A_s(R(T))$ is the attenuation per km for rain rate R(T). Persinger has shown that theoretically L_e is frequency dependant and this has been confirmed by observation. Figure 3.2-3 was plotted from data measured by Bostian et al [25]. Both signals were from the Comstar D2 satellite and therefore had the same physical path. In order to predict the attenuation at another frequency L_e must be scaled in some fashion. It is of interest that the best equation currently available for scaling attenuation from one frequency to another was derived assuming a nonuniform path [26].

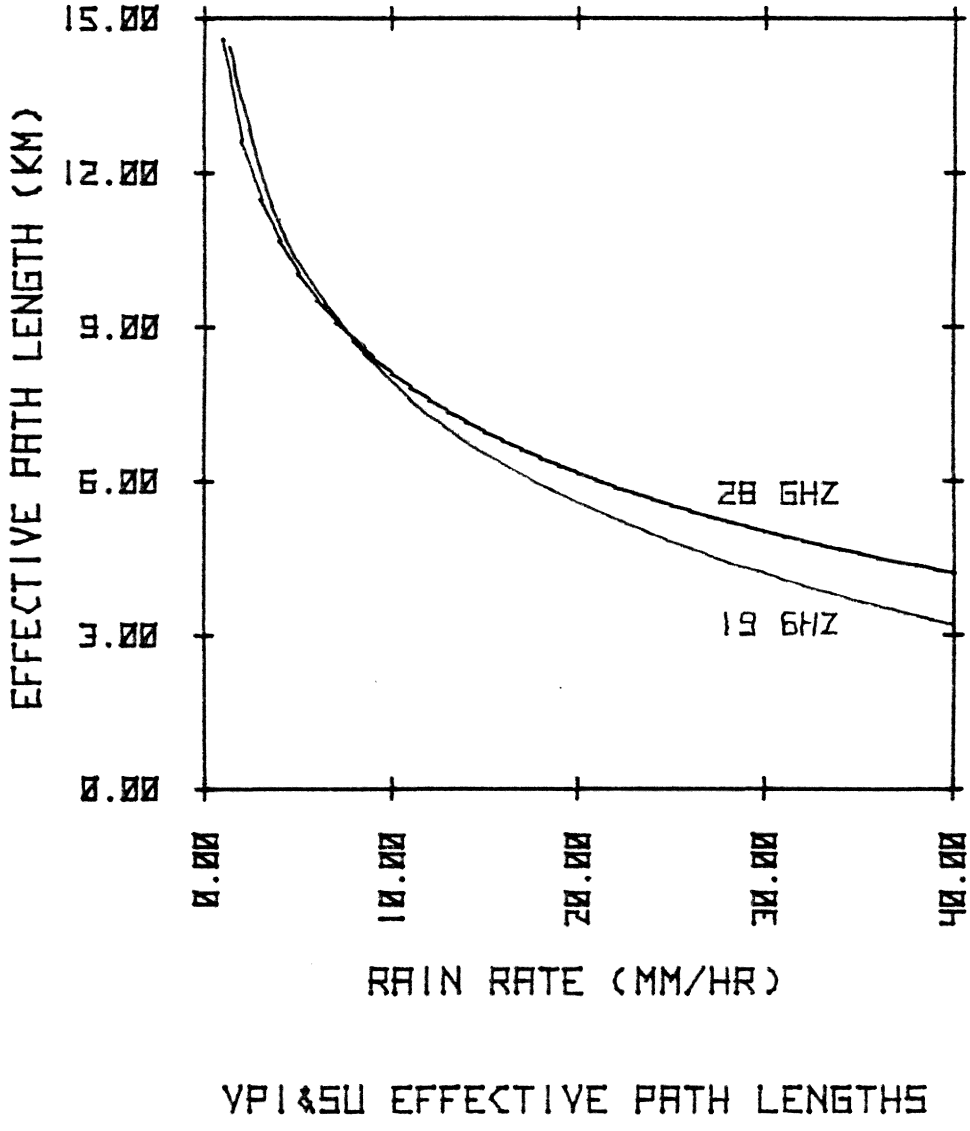

Figure 3.2-3. Effective path length L_e plotted vs rain rate. Measured at VPI&SU during July - September 1977.

The lack of correlation between L_e values measured at different locations is a more serious problem. The differences in effective path length are not explained by different elevation angles. Possible explanations are local terrain and climate differences but no method of accurately extrapolating L_e has been published.

The effective path length formulation of 3.2-1 does not allow the designer of a satellite system to accurately predict attenuation without on-site attenuation measurements. The models developed by Watson, Chu and Uzunoglu et al could be extended to a piecewise homogeneous path and the model developed by Persinger already has. However, admitting an inhomogeneous path raises the new problem of modeling the path. Though more work is needed in this area, a simple path model has been developed by the author and Persinger which yields quite good results. The development of this model is described in detail elsewhere [20] and only the results will be presented here.

The path model consists of a *storm extent* algorithm from which the path length L is determined and a *synthetic storm* algorithm which models the rain rate on the path. The storm extent algorithm is illustrated in Figure 3.2-4. The path length is determined by

$$L = \begin{cases} 10/\cos \alpha \text{ km} & \alpha \leq \tan^{-1}(\frac{6}{10}) \\ 6/\sin \alpha \text{ km} & \alpha > \tan^{-1}(\frac{6}{10}) \end{cases} \qquad (3.2\text{-}3)$$

where α is the elevation angle. L is independent of frequency and rain rate.

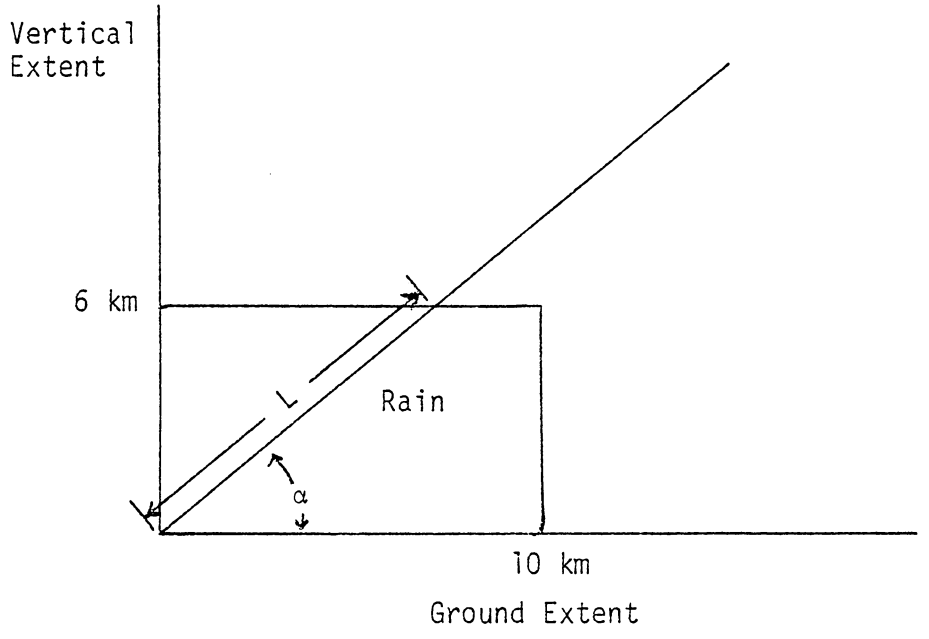

Figure 3.2-4. Storm extent algorithm.

The synthetic storm algorithm is illustrated in Figure 3.2-5. There are ten rain cells of width L/10. The rain rate in each cell is assumed to be uniform. Cell 1 is nearest the antenna and the rain rate in cell 1, R_1, is equal to the ground rain rate R. The rain rate in cells 2-10 is

$$R_i = R\left(\frac{R}{10}\right)^{X_i} \qquad \text{for} \qquad i = 2,3, \ldots 10 \qquad (3.2\text{-}4)$$

where

$$X_i = \begin{cases} 0 & \text{if } i = 2 \\ -0.66 & \text{otherwise} \end{cases} .$$

The general behavior of the rain rate distribution along the path is illustrated in Figure 3.2-5. It is important to note that the *shape* of the rain rate distribution is *rain rate dependant*. This more closely models the behavior of real rainfall. As the ground rain rate increases the area over which the higher rain rate exists decreases.

The rain path model was implemented with the Rain Propagation Prediction (RPP) program [20]. The RPP program contains all the state of the art refinements and can be used for any elevation angle and frequency. The results of the RPP program with the rain path model are compared with measured data from 3 locations in Figures 3.2-6 to 3.2-8. It must be noted that the measured data in the figures were used in the development of the rain path model. However

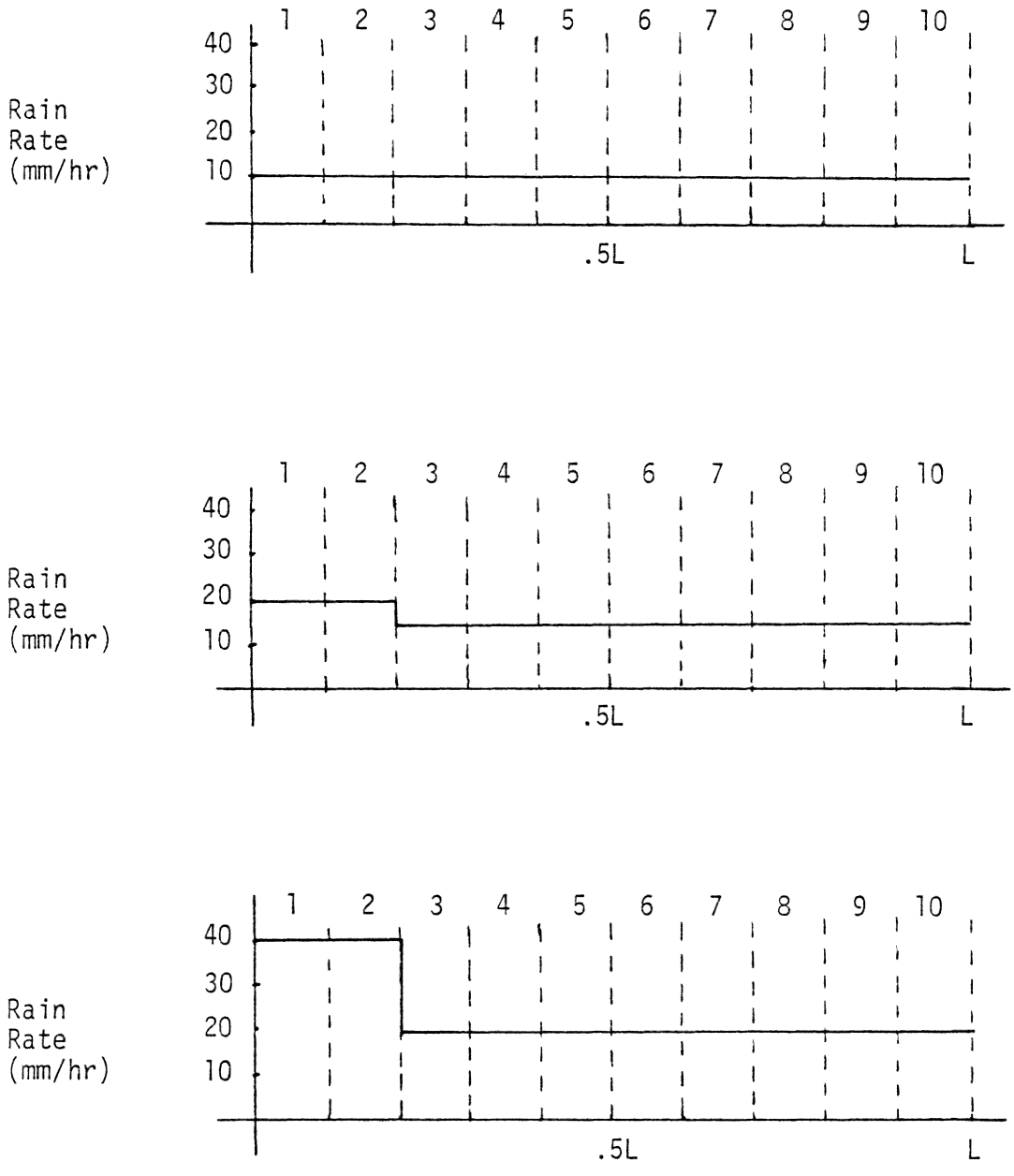

Figure 3.2-5. Synthetic storm algorithm.

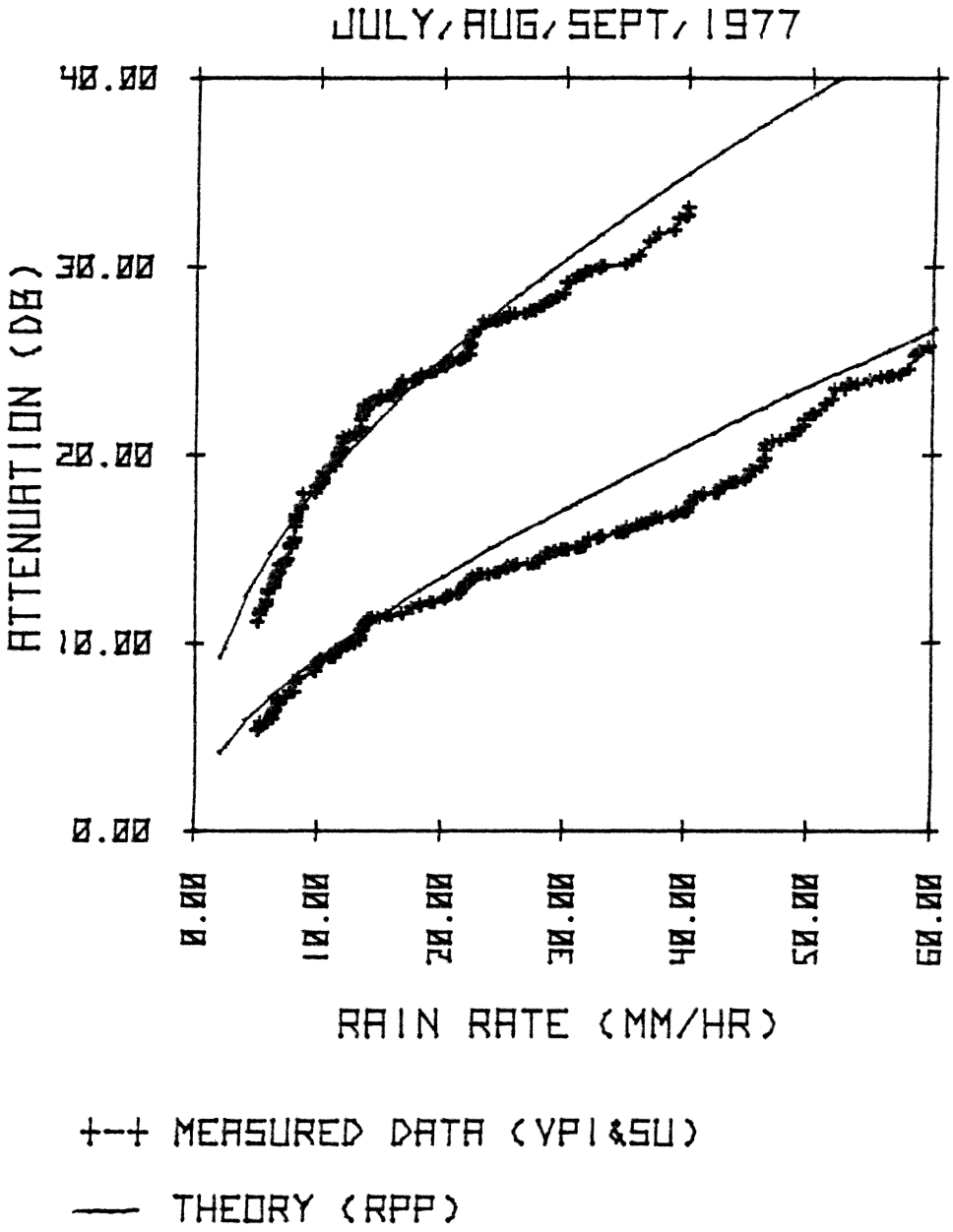

Figure 3.2-6. Measured attenuation at 28.56 and 19.04 GHz using the Comstar D2 satellite. Linear polarization, $\alpha = 44°$.

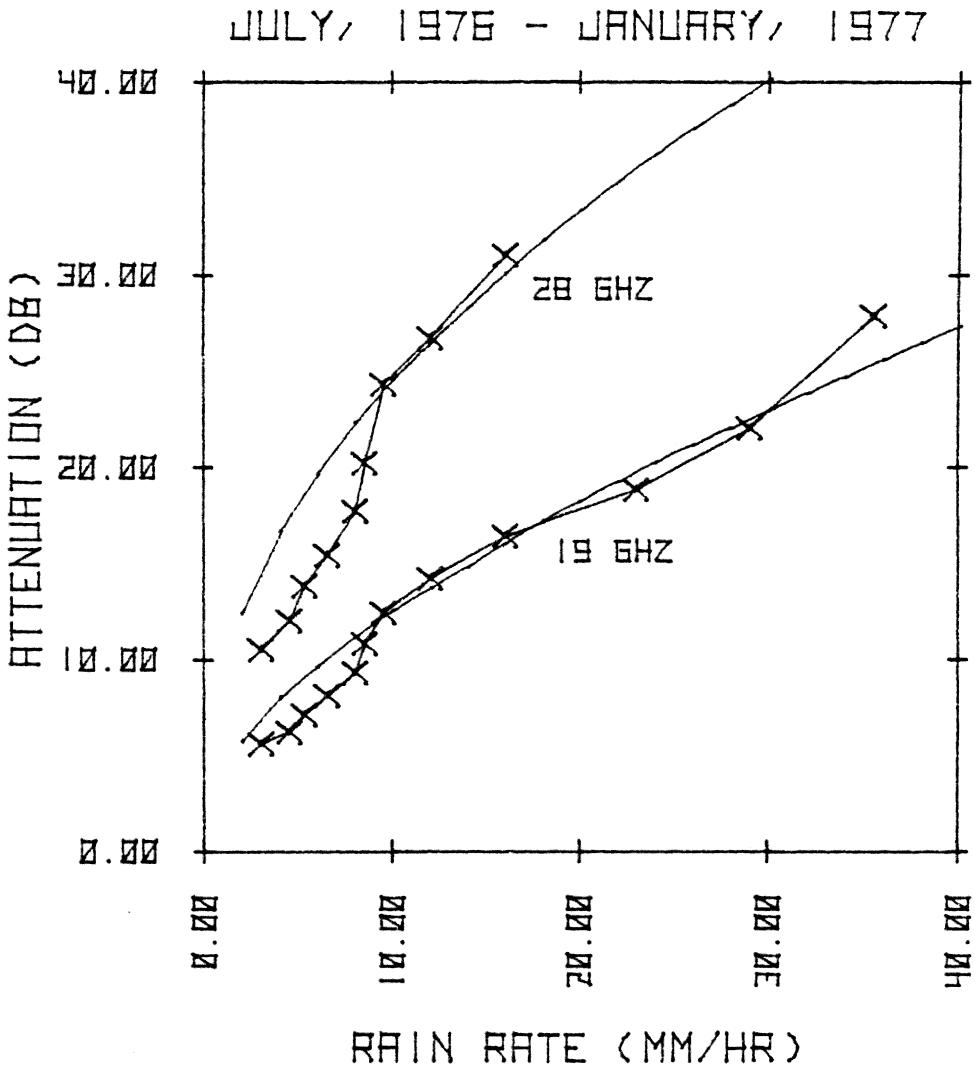

Figure 3.2-7. Measured attenuation at 28.56 and 19.04 GHz using the Comstar D1 satellite. Linear polarization, $\alpha = 23°$.

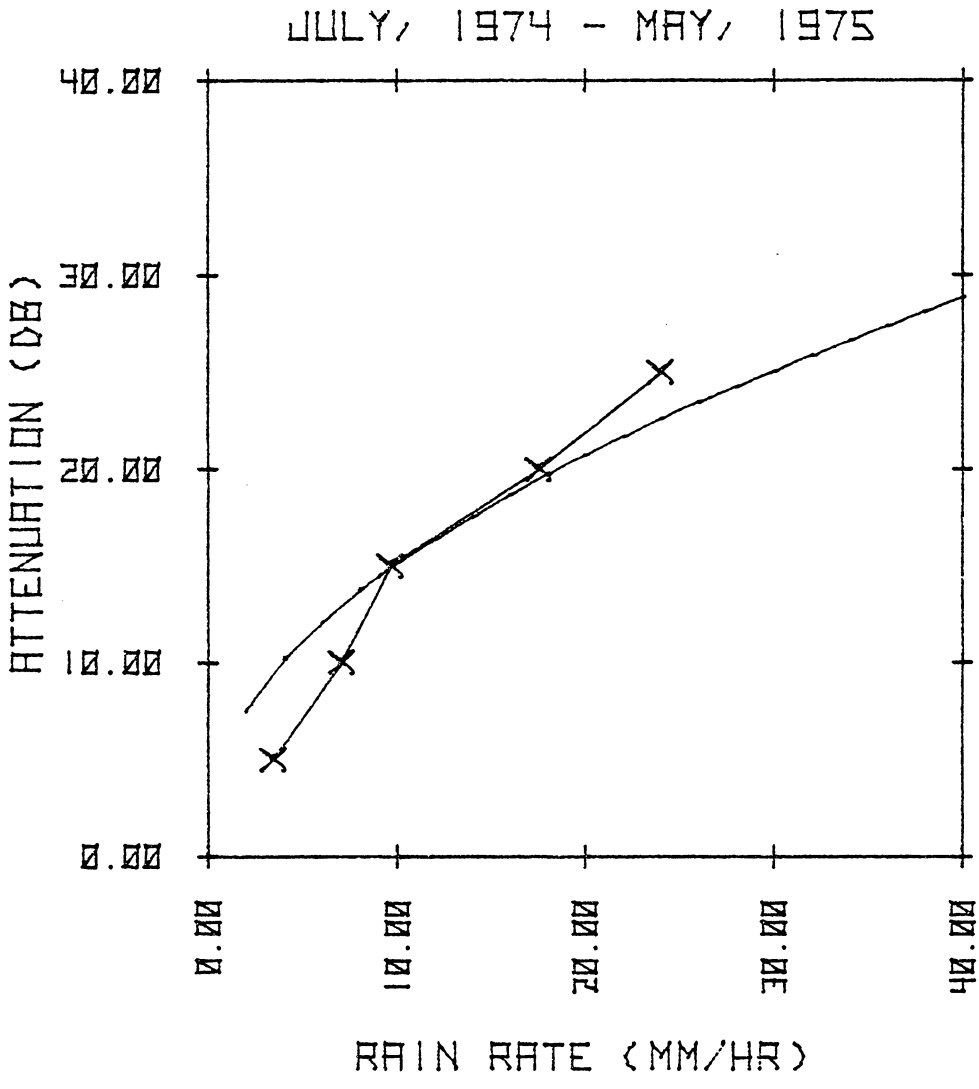

Figure 3.2-8. Measured attenuation data from University of Texas at Austin using the ATS-6 satellite. The frequency is 30 GHz, $\alpha = 54°$.

only two points at 30 GHz were used from the VPI&SU data [25], only one point at 30 GHz was used from the Comsat data [27] and only one point was used from the University of Texas at Austin data [28]. These points were used to determine the storm extent algorithm and no data measured at 20 GHz were used. The model extrapolates with frequency very well and a *maximum of one* measured data point is needed for extrapolation to other locations.

Equation 3.2-1 can be modified to include the synthetic storm algorithm. The result is

$$A(R) = \frac{L}{10} \sum_{i=1}^{10} A_s(R_i) \qquad (3.2\text{-}5)$$

where L is the path length, $A_s(R_i)$ is the attenuation per km for a rain rate R_i, and R_i is the rain rate in the ith cell computed from 3.2-4. Curve fits to A(R) and $A_s(R)$ are given in Chapter 5.

It is recognized that the storm extent algorithm and the synthetic storm algorithm are probably oversimplistic. The storm extent especially may need to be modified for different climatic zones. More work is needed in this area.

The verification of isolation predictions is more difficult due to the shortage of measured data. In Figures 3.2-9 and 10 the predictions of the RPP program are compared with the data measured at VPI&SU. The RPP curves were computed using the assumptions of 60% oblate raindrops and a 12° standard deviation of the canting angle. The agreement with the data is fairly good though the data has considerable scatter. Due to the limited verification at locations

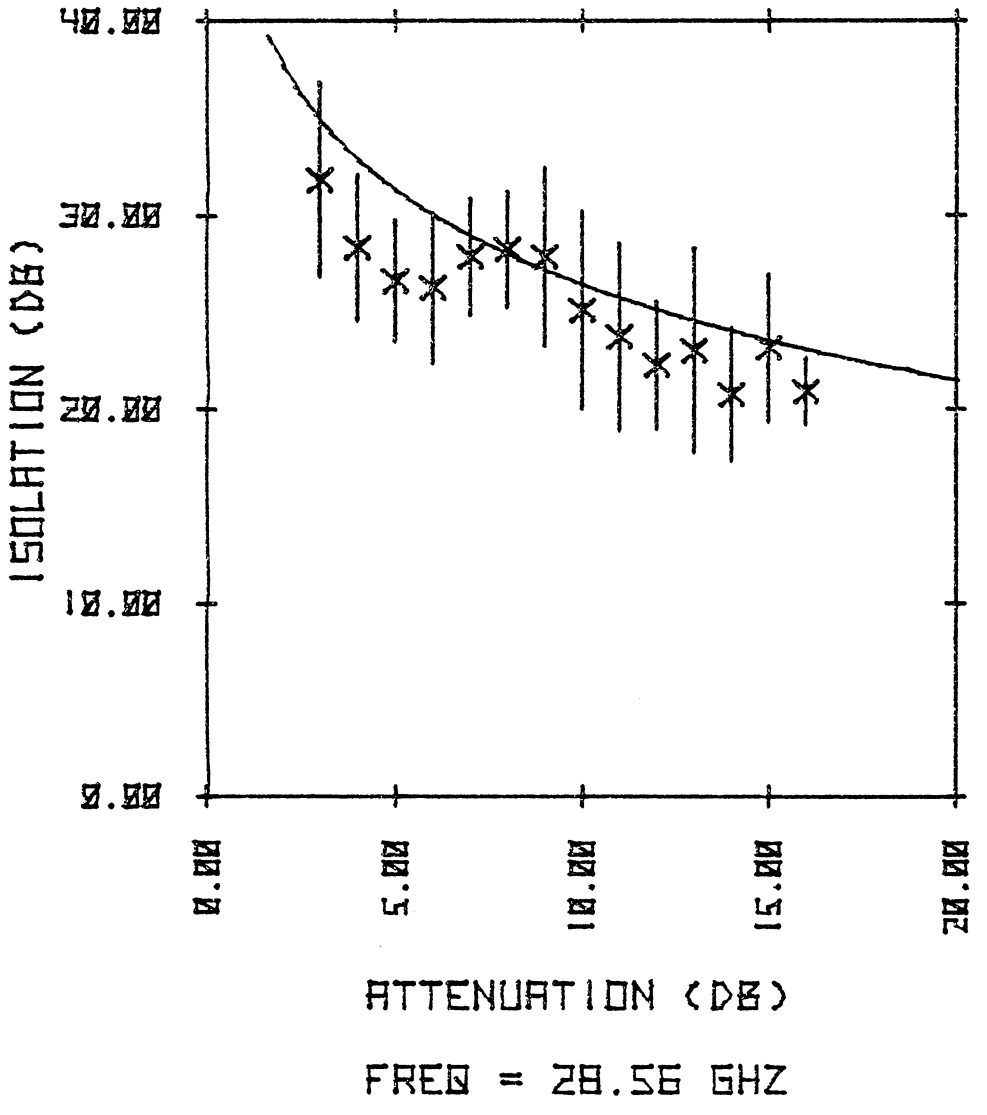

Figure 3.2-9. Isolation vs attenuation measured at VPI&SU using the Comstar D2 satellite. August 1977. Linear polarization.

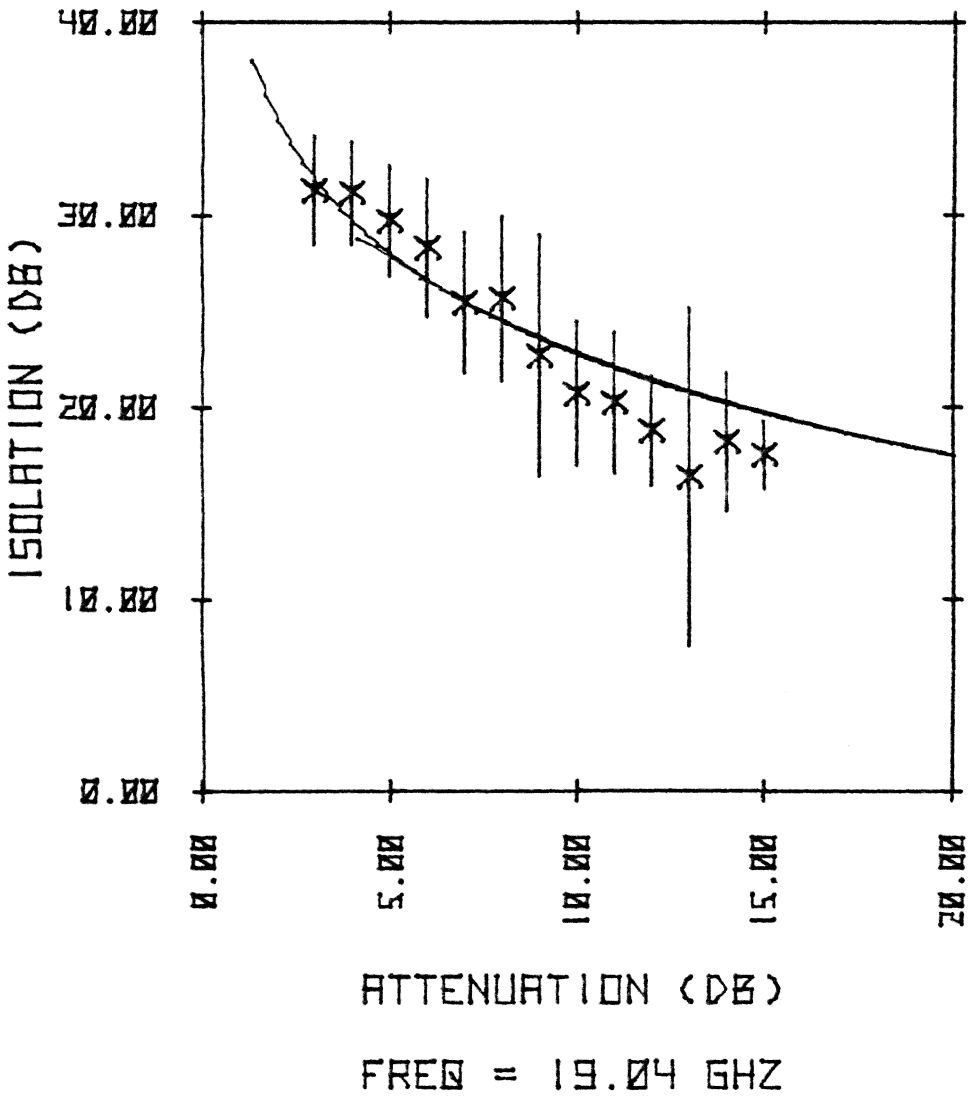

Figure 3.2-10. Isolation vs attenuation measured at VPI&SU using the Comstar D2 satellite. August 1977. Linear polarization.

other than VPI&SU the prediction of isolation may be questioned. However, as will be shown in Chapter 5, at 20 and 30 GHz depolarization is a second order effect compared to attenuation.

3.3 Rainfall Data

The results of the RPP program furnish the system designer with attenuation and isolation data as a function of ground rain rate. In addition the designer must know how often a given rain rate will be exceeded at the ground station. From this data the percent of time that a given margin is exceeded may be calculated. The rainfall data is best taken on the proposed site with fast response rain gauges for a period of one year or more. However this is often impractical. Rice and Holmberg [29] have developed a rain rate model which predicts the percent of time a given rain rate will be exceeded. This model is an empirical fit to a very large data base of rain accumulation in one-minute intervals, and to be strictly correct predicts the percent of one minute periods during which the rain rate averaged over one minute exceeded a given value. The Rice and Holmberg equation is given below.

$$\%T(R) = \frac{M}{T}(100)(0.03\ \beta\ e^{-0.03R} + .2(1 - \beta)(e^{-.258R} + 1.86\ e^{-1.63R})) \qquad (3.3\text{-}1)$$

where %T is the percent of time rain rate R will be exceeded, M is the total accumulation of rain in mm which fell in T hours, and β is

the "thunderstorm factor" which is the ratio of rainfall which fell during high rain rates to the total accumulation M. The total accumulation of rain measured at the VPI&SU tracking station during the year of 1977 was 620.8 mm (February was excluded due to equipment problems). From the curves published by Rice and Holmberg β is approximately 0.3. Equation 3.3-1 is plotted in Figure 3.3-1 along with measured data. The agreement is quite good.

If on site measurements are not available, National Weather Service data can be used with caution. The total accumulation measured by the NWS in Roanoke (approximately 60 km from VPI&SU) for the same time period was 776.3 mm. Equation 3.3-1 is plotted in Figure 3.3-2 using this value of M. The results are still good. However the local NWS observer located only 8 km from VPI&SU has consistantly measured much more rainfall than VPI&SU. Local terrain differences are believed to be responsible.

The Rice and Holmberg model allows rain rate statistics to be estimated from on-site or NWS measurements. Once the rain rate distribution is known the attenuation and depolarization for a given rain rate can be calculated to yield percent of time distributions for attenuation and depolarization. For a given system margin the percent of time the link is unavailable may be calculated.

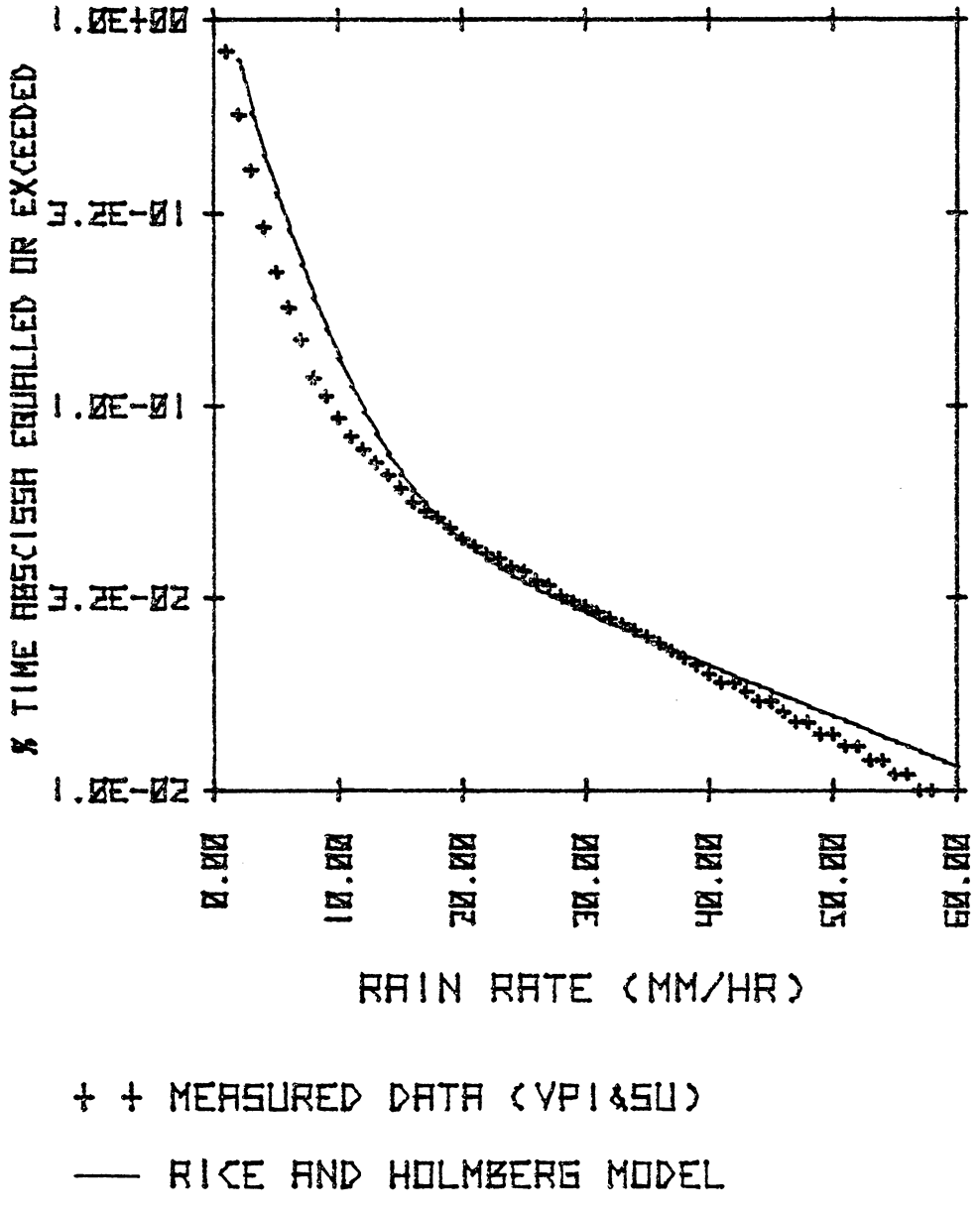

Figure 3.3-1. VPI&SU rain rate statistics compared with the Rice and Holmberg model (equation 3.3-1) using the VPI&SU measured accumulation.

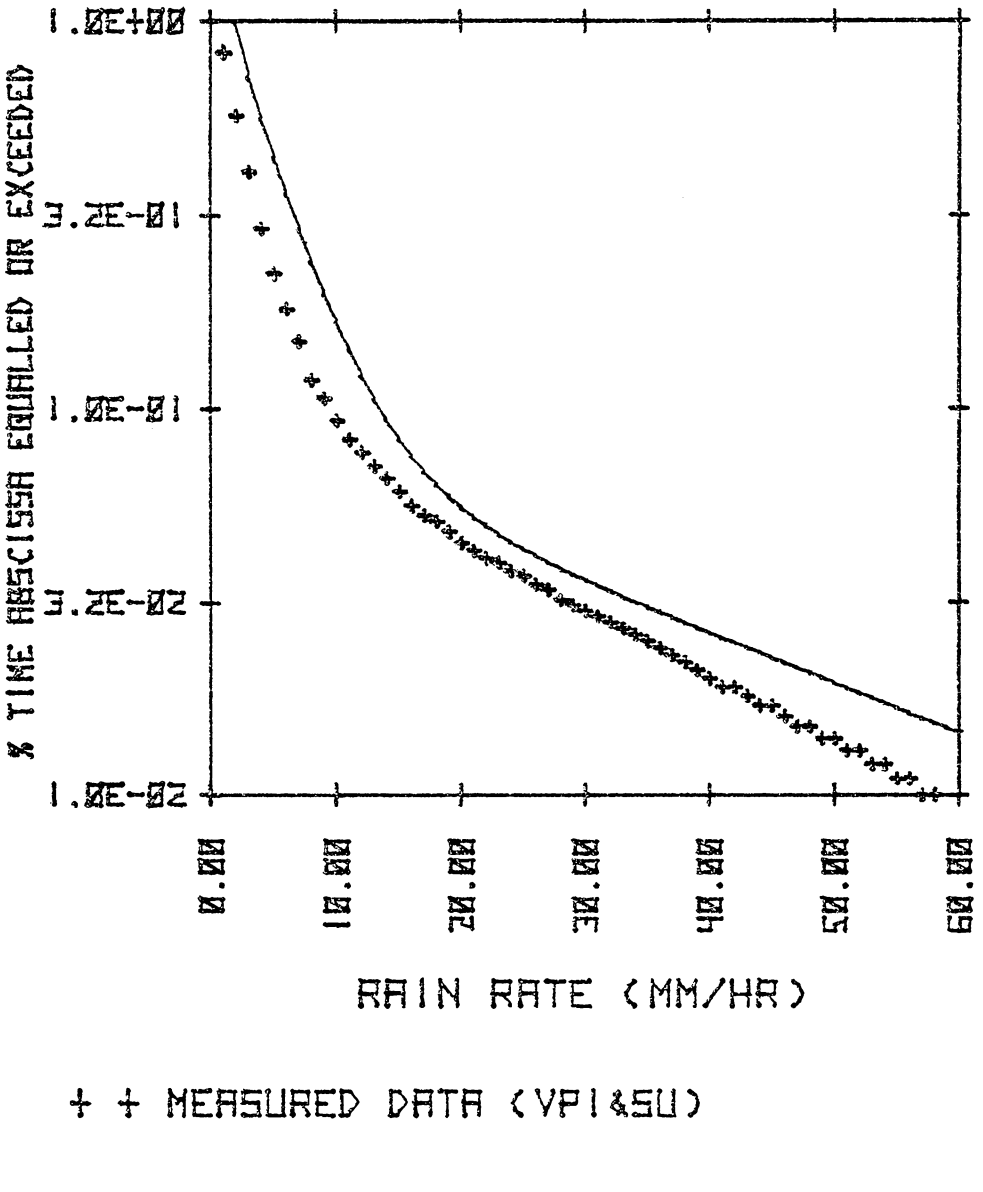

Figure 3.3-2. VPI&SU rain rate statistics compared with the Rice and Holmberg model (equation 3.3-1) using the NWS measured accumulation.

CHAPTER 4

ANTENNA EFFECTS

A communications system employing orthogonal polarization frequency reuse requires high-purity dual polarized antennas that maintain a 30 dB isolation between the two channels (see Figure 2.3-2). There is no problem meeting this requirement on antenna boresight where the ground antenna is normally operated. Off boresight the polarization purity is less and the isolation is degraded. Off boresight operation is caused by antenna mispointing (except for low elevation angles where multipath effects may be significant). Pointing requirements imposed by dual polarized operation will be examined.

Many systems (including the MWCE) are planned with circular polarization. A real antenna does not transmit perfect circular polarization but elliptical. Best isolation is attained when the major axis of the wave and the cross-polarized receive antenna state are perpendicular. The improvement attained by major axis alignment will be examined and an assessment made of its desirability.

4.1 Pointing Accuracy

Theoretical work on off-axis polarization purity of paraboloidal antennas has been done by Watson and Ghobrial [30]. Their conclusion is that for dual polarized use the cassergrain is much preferred over the prime focus configuration. This occurs because of the

partial cancellation of cross polarized fields by the subreflector in the cassegrain system. Watson and Ghobrial's calculations indicate that maintaining 30 dB of isolation between the dual channels requires that a cassegrain antenna be operated within the half power beamwidth and a prime focus antenna be operated within approximately 0.25 x the half power radius.

This relatively poor performance of the prime focus antenna off axis has not been observed. A prime focus antenna is used at VPI&SU to receive a beacon signal from the Comstar D2 satellite. This antenna has fixed pointing and satellite motion has caused diurnal variations in the received signal level of 4 dB. This 4 dB variation means the antenna was mispointed so as to place the satellite outside the half power beamwidth. The isolation showed a diurnal variation of 8 dB but never fell below 27 dB (clear weather).

The predictions of Watson and Ghobrial appear to be pessimistic though their conclusion that the cassegrain is superior in dual polarized use is not doubted. Nevertheless, the isolation of a prime focus antenna is sufficient for dual polarized use as long as the pointing is within the half power beamwidth. Normally an antenna, cassegrain or prime focus, will be pointed to that accuracy anyway and no further requirements on pointing for dual polarized use are forseen.

4.2 Polarization Tracking

A "circularly" polarized antenna is really elliptically polarized

with some axial ratio AR and tilt angle τ as illustrated in Figure 4.2-1. Consider an incoming wave (from a non-perfect antenna) with an axial ratio AR_W and tilt angle τ_W. The dual polarized ground station antenna has a *co-polarized* state AR_C, τ_C which is designed to achieve maximum coupling with the incident wave. The ground antenna's cross-polarized state AR_X, τ_X is designed for minimum coupling with the incident wave. Ideally $AR_C = AR_W = -AR_X$ and $\tau_C = \tau_W = \tau_X \pm 90°$ where the negative axial ratio signifies opposite sense of rotation. In practice AR_C may not be $-AR_X$ and τ_C may not be $\tau_X \pm 90°$ but they will usually be close. Isolation is the ratio of the power coupled to the co-polarized antenna state to the power coupled to the cross-polarized state. The isolation I can be expressed as [31]

$$I = \frac{\left[\dfrac{(AR_W^2 + 1)(AR_C^2 + 1) + 4\,AR_W\,AR_C + (AR_W^2 - 1)(AR_C^2 - 1)\cos 2\,\Delta\tau_C}{2(AR_W^2 + 1)(AR_C^2 + 1)}\right]}{\left[\dfrac{(AR_W^2 + 1)(AR_X^2 + 1) + 4\,AR_W\,AR_X + (AR_W^2 - 1)(AR_X^2 - 1)\cos 2\,\Delta\tau_X}{2(AR_W^2 + 1)(AR_X^2 + 1)}\right]} \qquad (4.2\text{-}1)$$

where $\Delta\tau_C = \tau_C - \tau_W$ and $\Delta\tau_X = \tau_X - \tau_W$. The maximum isolation is achieved for $\Delta\tau_C = 0$ and $\Delta\tau_X = 90°$. Assuming an $AR_W = 0.5$ dB [1] and $AR_C = -AR_X = 0.4$ dB the maximum and minimum isolations are 44.8 and 25.7 dB respectively. For a synchronous satellite τ_C and τ_X can be manually adjusted for maximum isolation. However, for the MWCE the

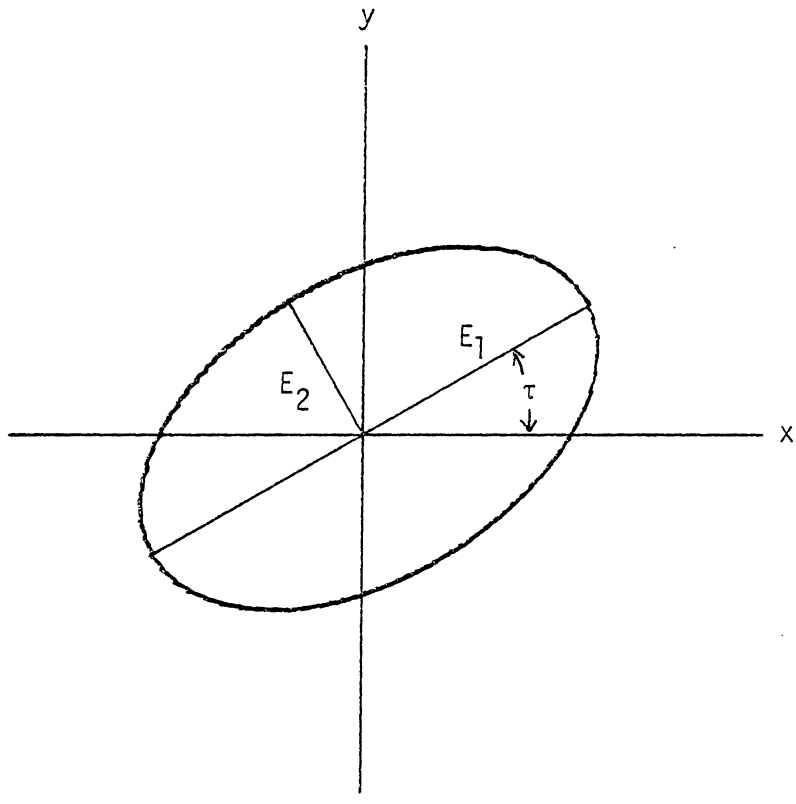

$$AR = \frac{E_1}{E_2}$$

Figure 4.2-1. Polarization ellipse.

tilt angle τ_W would be changing as the spacecraft passes overhead and would have to be actively tracked to achieve maximum isolation. The degradation in CNR caused by an isolation of 25.7 dB is only 0.6 dB (see Chapter 2) and the minor improvement attainable is not worth the effort (if the MWCE polarization were linear τ_W would *have* to be tracked).

In general rain on the propagation path will change both AR_W and τ_W. Tracking τ_W will yield an improvement in isolation but investigation with the RPP program (see Chapter 3) has shown the improvement in CNR degradation to be less than 1 dB for both 20 and 30 GHz. This improvement is probably too small to be worth the effort of tracking τ_W. However, should linear polarization be used, the improvement in CNR degradation appears quite substantial.

CHAPTER 5

SYSTEM CALCULATIONS

The effects of crosstalk between the channels of a dual polarized communications link have been calculated in Chapter 2 and the effects of rain taken up in Chapter 3. Antenna effects were shown to be negligible in Chapter 4 (except for possible pointing loss). System calculations can now be made to assess operating margins, G/T and EIRP requirements, and the percent of time that the link will be unavailable. Calculations will be done using the system parameters of the MWCE, but the methods are applicable to any digital communications system, either dual or single polarized.

5.1 Clear Weather System Calculations

The design goal for a MWCE tracking station is 10 dB margin at a 5° elevation angle in the transponder mode of operation. In the transponder mode the uplink is simply translated to 20 GHz and downlinked to the same tracking station by the spacecraft. This allows BER and channel cross correlation measurements to be made easily. The required G/T and EIRP of the ground station for transponder mode operation will now be calculated.

Because the uplink (30 GHz) attenuation caused by rain is approximately twice the downlink (20 GHz) attenuation [25], the uplink margin will be set equal to twice the downlink margin (the choice of 2 also simplifies the equations considerably as will be

seen). The total CNR for transponder operation can be expressed as follows:

$$\left(\frac{C}{N}\right) = \frac{1}{\frac{1}{\left(\frac{C}{N}\right)_u} + \frac{1}{\left(\frac{C}{N}\right)_d}} \qquad (5.1\text{-}1)$$

where C/N is the carrier to noise power ratio (not in dB). Let K be the required total C/N and m_u, m_d and m_t the uplink, downlink and total margins (not in dB) respectively. Equation 5.1-1 can then be written as

$$m_t K = \frac{1}{\frac{1}{m_u K} + \frac{1}{m_d K}} \qquad (5.1\text{-}2)$$

$$\frac{1}{m_t} = \frac{1}{m_u} + \frac{1}{m_d} \quad . \qquad (5.1\text{-}3)$$

For an uplink margin twice the downlink, $M_u = 2\ M_d$, $10 \log_{10} M_u = 2 \times 10 \log_{10} M_d$ or $m_u = m_d^2$ and 5.1-3 can be written as

$$\frac{1}{m_t} = \frac{1}{m_d} + \frac{1}{m_d^2} \quad . \qquad (5.1\text{-}4)$$

The total margin is 10 dB, or $m_t = 10$; therefore,

$$0.1 = \frac{1}{m_d} + \frac{1}{m_d^2} \quad . \qquad (5.1\text{-}5)$$

or

$$0.1\ m_d^2 - m_d - 1 = 0 \quad . \qquad (5.1\text{-}6)$$

Use of the quadratic formula yields

$$m_d = 10.92$$

and in dB the margins are

$$M_d = 10.38 \text{ dB} \qquad M_u = 20.76 \text{ dB} \quad .$$

The required CNR is calculated from the requirement of 10^{-5} BEP [1]. The BEP is the P_u of Chapter 2 and can be written as

$$\text{BEP} = \frac{1}{2}\,\text{erfc}\left(\frac{\rho}{\sqrt{2}}\right) \tag{5.1-7}$$

where $\rho = 10^{\text{CNR}/20}$. Equation 5.1-7 can be solved for ρ and the required CNR is 12.6 dB. Assorted hardware problems will degrade this theoretical performance by 3.1 dB so the required CNR is 15.7 dB [1].

The distance from a ground station to a spacecraft in a circular orbit as a function of station elevation angle is derived in the Appendix. The result is

$$d_{sc} = \cos\left[\sin^{-1}\left[\frac{R}{R_e + h_{sc}}\cos(\alpha)\right] + \alpha\right]\frac{R_e + h_{sc}}{\cos(\alpha)} \tag{5.1-8}$$

where α is the elvation angle, R_e is the radius of the earth (6377 km) and h_{sc} is the height of the orbit. For h_{sc} = 400 km and $\alpha = 5°$, d_{sc} is 1804 km. The free space loss can be calculated from

$$L_f = 20 \log d + 20 \log f + 92.44 \text{ dB} \tag{5.1-9}$$

where d is the distance in km and f is the frequency in GHz.

$$L_f(20 \text{ GHz}) = 183.6 \text{ dB}$$

and

$$L_f(30\ \text{GHz}) = 187.1\ \text{dB} \quad .$$

From Chapter 3 the atmospheric loss is

$$L_a = \frac{A_z}{\sin \alpha}$$

$$A_z = \begin{cases} 0.45 & f = 20\ \text{GHz} \\ 0.33 & f = 30\ \text{GHz} \end{cases} \qquad (5.1\text{-}10)$$

$$L_a(20\ \text{GHz}) = 5.16\ \text{dB}$$

$$L_a(30\ \text{GHz}) = 3.79\ \text{dB}$$

where $\alpha = 5°$. The received CNR can be written as

$$\text{CNR} = \text{EIRP} - L_T + G/T - K - B \qquad (5.1\text{-}11)$$

where;

EIRP is effective radiated power, dBW

L_T is the total loss, dB

G/T is receive antenna gain over system noise temperature, dB/K

K is Boltzman's constant, -228.6 dBW/K Hz

B is the symbol rate bandwidth, dBHz .

The received CNR = 15.7 + M where M is the margin and the ground

station G/T and EIRP may now be calculated. Rewriting 5.1-11 and using the subscripts G for ground station. SC for spacecraft, d for downlink and u for uplink yields

$$(G/T)_G = 15.7 + M_d - EIRP_{SC} + L_{Td} + K + B \qquad (5.1\text{-}12)$$

$$EIRP_G = 15.7 + M_u + L_{Tu} - (G/T)_{SC} + K + B \quad . \qquad (5.1\text{-}13)$$

Substituting $M_d = 10.38$, $EIRP_{SC} = 48.5$, $L_{Td} = 183.6 + 5.2 + 0.5$ (pointing loss), $K = -228.6$ and $B = 84.0$ (50 Mbps or 25 M symbols per sec.) yields

$$(G/T)_G = 22.3 \text{ dB/K} \quad .$$

Similarly with $M_u = 20.76$, $G/T_{SC} = 4.4$ and $L_{Tu} = 187.1 + 3.8 + 0.5$ (pointing loss)

$$EIRP_G = 78.86 \text{ dBW} \quad .$$

The link calculations are summarized in Table 5.1-1.

VPI&SU already has an excellent 12 foot fully steerable dish which could be adapted for 20/30 GHz operation. Assuming an aperture efficiency of 55% the gain of the dish would be 58.6 dB at 30 GHz and 55.1 dB at 20 GHz. To realize the EIRP requirement, the required input power to the antenna would be 106 watts. To realize the G/T requirement, the system noise temperature referenced to the antenna port would have to be 32.7 dBK or 1860 K.

Table 5.1-1. Link Calculations

		UPLINK		DOWNLINK
1.	Frequency (GHz)	30		20
2.	EIRP (dBW)	78.9		48.5
3.	Losses			
	Free Space Loss (dB)	187.1		183.6
	Atmospheric Loss (dB)	3.8		5.2
	Pointing Loss (dB)	0.5		0.5
	Polarization Loss (dB)	0.0		0.0
	Total Losses (dB)	191.4		189.3
4.	G/T (dB/K)	4.4		22.3
5.	Symbol Rate Bandwidth (dBHz)	84.0		84.0
6.	Boltzman's Constant (dB/Hz K)	-228.6		-228.6
7.	CNR (dB)	36.5		26.1
8.	Total CNR (dB)		25.7	
9.	Bit Sync. Degr. (dB)		3.1	
10.	Required CNR (dB)		12.6	
11.	Margin (dB)		10.0	

Notes for Table 5.1-1

1. Given.
2. Uplink calculated in text, downlink [1].
3. Free space calculated in text, atmospheric calculated in text, pointing loss [1], polarization loss [31]

$$Loss_{pol} = 10 \log_{10} \left(\frac{1}{2} + \frac{4AR_w AR_a - (AR_w^2 - 1)(AR_a^2 - 1)}{2(AR_w^2 + 1)(AR_a^2 + 1)}\right)$$

where $AR_w = 10^{0.5/20}$, $AR_a = 10^{0.4/20}$. This equation is worst case.

4. Uplink [1], downlink calculated in text.
5. [1]
6. $10 \log_{10}(1.38 \times 10^{-23})$
7. (2) - (3) + (4) - (5) - (6)
8. Equation 5.1-1.
9. [1]
10. Calculated in text, equation 5.1-7.
11. (8) - (9) - (10)

5.2 The Effects of Rain on the System

With the clear weather margins established, the effects of rain on the system can be evaluated. The attenuation of the signal by rain is computed using the RPP program [20] as outlined in Chapter 3. The results of the program will be expressed as

$$A_R = aR^b \qquad (5.2\text{-}1)$$

where R is the ground rain rate and A_R is the total path attenuation in dB. The coefficients a and b are determined from the results of the RPP program by curve fitting. The correlation coefficient, R^2, was 0.98 or better for all cases. An R^2 of 1.00 means the fit was perfect. The coefficients a and b are tabulated in Table 5.2-1 for various elevation angles.

Evaluation of the depolarization effects of rain are most easily done with the RPP results in the form

$$I = u + v \log_e(R) \qquad (5.2\text{-}2)$$

where I is the channel isolation in dB and R is the ground rain rate in mm/hr. The coefficients u and v were determined by curve fitting and are also tabulated in Table 5.2-1. The values of R^2 were 0.98 or higher for all values of α less than 70°. Above 70° the values of R^2 dropped sharply, but for elevation angles above 70° the depolarization is negligible. Antenna effects were included in these results.

Should the synthetic storm or storm extent algorithms be

Table 5.2-1. Path attenuation and isolation curve fit coefficients based on storm extent and synthetic storm models. Circular polarization.

20 GHz

α	a	b	u	v
5	3.207	0.546	29.750	-5.159
10	3.240	0.547	29.856	-5.162
15	3.302	0.548	29.794	-5.111
20	3.388	0.549	30.286	-5.173
25	3.507	0.551	30.371	-5.122
30	3.664	0.553	31.050	-5.192
35	3.309	0.555	33.602	-5.323
40	2.940	0.558	35.580	-5.319
45	2.673	0.560	37.563	-5.258
50	2.456	0.563	41.129	-5.538
55	2.295	0.565	43.181	-5.389
60	2.166	0.567	48.612	-5.987
65	2.069	0.568	50.024	-5.417
70	1.995	0.570	58.107	-6.117
75	1.937	0.571	52.867	-3.184
80	1.898	0.572	42.629	3.108
85	1.876	0.572	41.579	1.324
90	1.869	0.572	44.784	0

Table 5.2-1 (continued). Path attenuation and isolation curve fit coefficients based on storm extent and synthetic storm models. Circular polarization.

30 GHz

α	a	b	u	v
5	7.750	0.448	24.076	-3.702
10	7.844	0.449	24.183	-3.706
15	8.013	0.449	24.320	-3.704
20	8.256	0.450	24.611	-3.720
25	8.586	0.451	24.908	-3.722
30	9.020	0.452	25.369	-3.744
35	8.197	0.454	28.353	-3.979
40	7.333	0.456	29.821	-3.873
45	6.697	0.457	32.230	-3.914
50	6.205	0.458	35.179	-4.051
55	5.833	0.459	38.143	-4.117
60	5.536	0.460	42.417	-4.446
65	5.315	0.461	46.900	-4.630
70	5.146	0.462	57.199	-6.178
75	5.014	0.462	62.023	-5.263
80	4.926	0.463	50.383	0.830
85	4.874	0.463	42.902	2.050
90	4.861	0.463	44.775	0

modified to better fit local conditions, attenuation can be computed from

$$A(R) = \frac{L}{10} \sum_{i=1}^{10} A_s(R_i) \qquad (5.2\text{-}3)$$

where L is the path length in km (see equation 3.2-3), R_i is the rain rate in cell i (see equation 3.2-4) and A_s is the attenuation per km. A_s is given as an εR^{ζ} curve fit. Values of ε and ζ for circular polarization are listed in Table 5.2-3. ε and ζ are functions of polarization, canting angle distribution, drop size distribution, elevation angle and frequency. Values are available in the literature [32] but care should be taken to compute A_s for the parameters of the system in question. It must also be noted that εR^{ζ} is a curve fit to calculation and is not exact. Isolation may be calculated from curve fits of the form $I = c + d \log_e(A)$ where A is the rain induced attenuation in dB. The coefficients c and d are listed in Table 5.2-4.

Once the attenuation and isolation are determined their effects on the system performance are best described by an *effective* attenuation. This effective attenuation, A_{eff} is defined as

$$A_{eff} = A_R + D_R \qquad (5.2\text{-}4)$$

where A_R is the attenuation caused by rain from 5.2-1 and D_R is the *degradation* in CNR caused by crosstalk. Isolation for a dual polarized system is the same as the carrier to interference ratio (CIR) of Chapter 2. Therefore the final results of Chapter 2 are

Table 5.2-2. Specific attenuation coefficients, circular polarization, mean canting angle, 0; canting angle standard deviation, 12°.

	20 GHz		30 GHz	
α	ε	ζ	ε	ζ
5	0.0906	1.0712	0.2525	0.9087
10	0.0904	1.0722	0.2526	0.9093
15	0.0903	1.0737	0.2528	0.9101
20	0.0900	1.0758	0.2531	0.9113
25	0.0897	1.0783	0.2535	0.9128
30	0.0894	1.0813	0.2539	0.9145
35	0.0890	1.0845	0.2544	0.9163
40	0.0886	1.0879	0.2550	0.9182
45	0.0882	1.0914	0.2555	0.9202
50	0.0878	1.0948	0.2561	0.9221
55	0.0875	1.0980	0.2567	0.9239
60	0.0871	1.1011	0.2572	0.9255
65	0.0868	1.1038	0.2577	0.9270
70	0.0866	1.1061	0.2582	0.9283
75	0.0864	1.1080	0.2585	0.9293
80	0.0862	1.1094	0.2588	0.9301
85	0.0861	1.1102	0.2590	0.9306
90	0.0861	1.1106	0.2590	0.9307

Table 5.2-3. Isolation vs attenuation curve fit coefficients, circular polarization, mean canting angle 0, canting angle standard deviation 12°, 60% oblate drops.

	20 GHz		30 GHz	
α	c	d	c	d
5	38.70	-9.15	41.44	-8.28
10	38.89	-9.14	41.64	-8.27
15	39.23	-9.13	41.99	-8.26
20	39.71	-9.11	42.48	-8.25
25	40.35	-9.09	43.13	-8.24
30	41.16	-9.06	43.94	-8.22
35	42.14	-9.04	44.93	-8.21
40	43.32	-9.01	46.12	-8.19
45	44.72	-8.98	47.54	-8.18
50	46.38	-8.96	49.22	-8.16
55	48.37	-8.93	51.21	-8.14
60	50.75	-8.90	53.60	-8.13
65	53.65	-8.88	56.51	-8.12
70	57.28	-8.86	60.15	-8.10
75	62.03	-8.84	64.92	-8.09
80	68.76	-8.82	71.67	-8.08
85	80.08	-8.76	83.05	-8.06
90	115.41	-2.42	117.84	-1.58

used to calculate D_R as follows

$$D_R = -20 \log_{10}(1 - \sqrt{2}\, F) \qquad (5.2\text{-}5)$$

where $F = 10^{-I/20}$ and I is the isolation from 5.2-2. By the use of equation 5.2-1, 2, 4 and 5 the effective attenuation A_{eff} can be calculated. A_{eff} represents the actual system impact of rain attenuation and depolarization. Effective attenuation is plotted as a function of rain rate in Figure 5.2-1 through 4 for elevation angles of 5, 30, 45 and 60 degrees. The curves labeled D are the A_{eff} for a dual polarized system and the curves labeled S are for a single polarized system. The degradation resulting from depolarization for a single polarized system is zero, and $A_{eff} = A_R$.

A_{eff} for a dual polarized system is only one to three dB greater than that for a single polarized system at 5 and 30 degrees elevation angle and for higher elevation angles the difference is even less. This shows that a dual polarized system will "cost" only one to three dB more in margin than a single polarized system with the same reliability. The depolarization caused by rain is a minor effect compared to attenuation. This is not true at lower frequencies where significant depolarization can occur with much less attenuation.

The use of a suitable rain rate model will allow the percent of time a given effective attenuation will be exceeded to be calculated. The Rice and Holmberg model [29] discussed in Chapter 3 has agreed very well with the rain rate data measured at VPI&SU (refer to section 3.3). The Rice and Holmberg equation can be written as

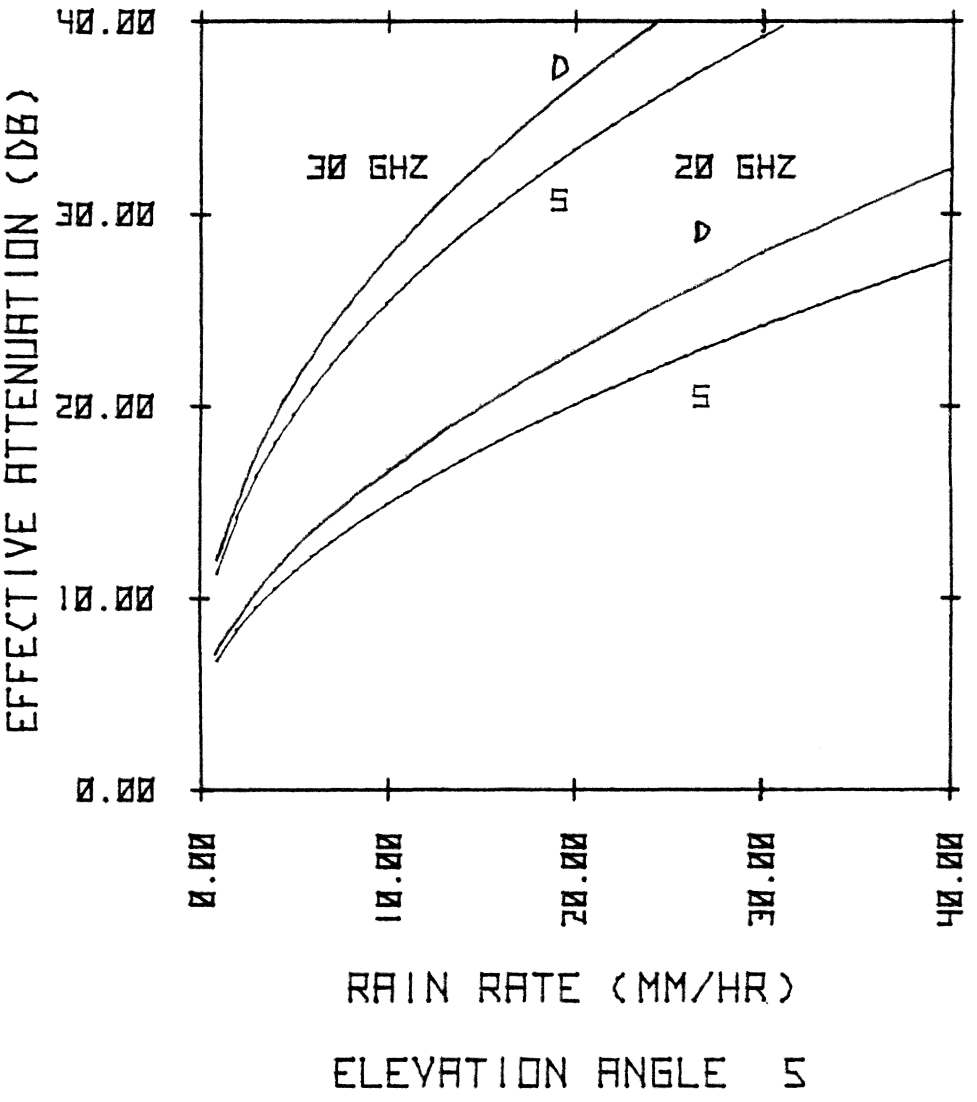

Figure 5.2-1. Effective attenuation (A_{eff}) for a dual (D) and single (S) polarized system as a function of rain rate.

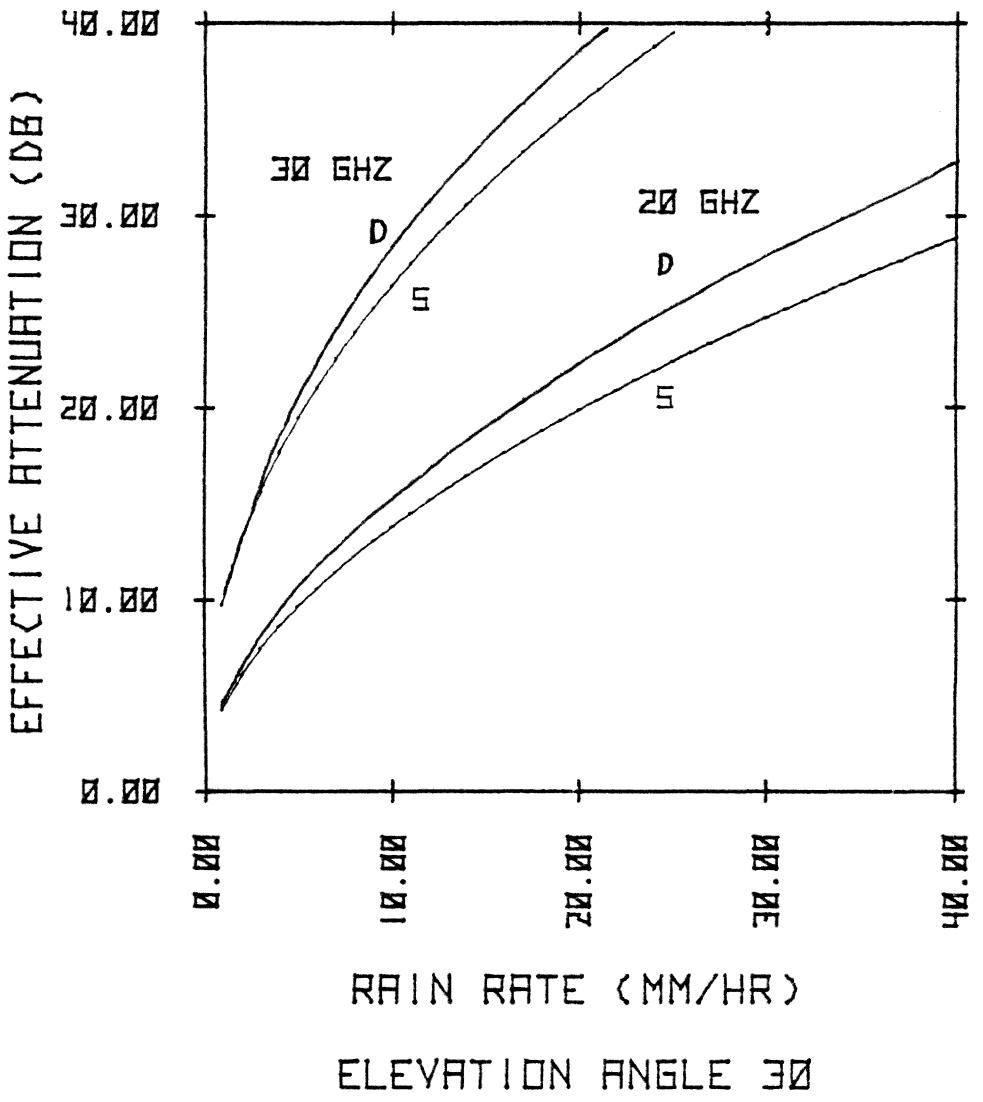

Figure 5.2-2. Effective attenuation (A_{eff}) for a dual (D) and single (S) polarized system as a function of rain rate.

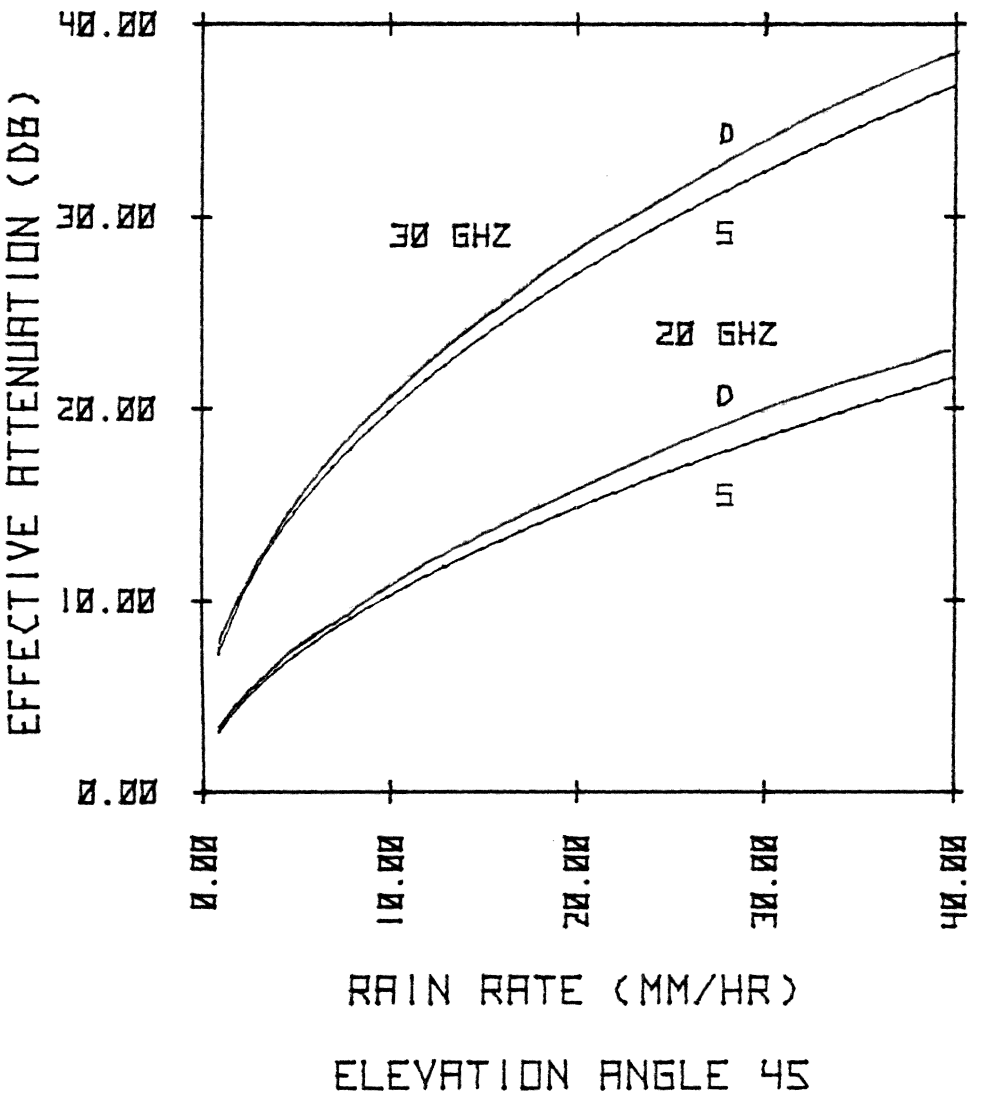

Figure 5.2-3. Effective attenuation (A_{eff}) for a dual (D) and single (S) polarized system as a function of rain rate.

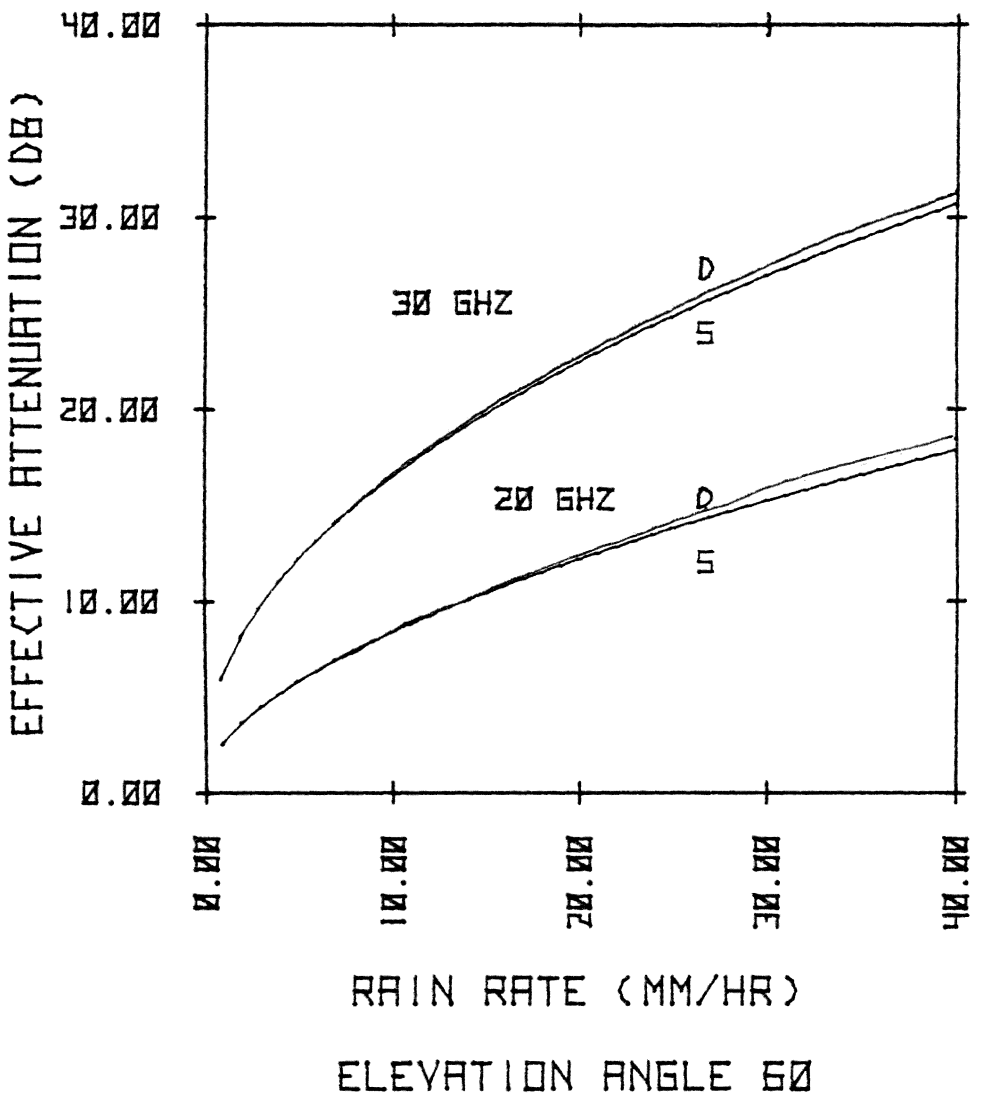

Figure 5.2-4. Effective attenuation (A_{eff}) for a dual (D) and single (S) polarized system as a function of rain rate.

$$\%T = \frac{M}{T}\left(0.03\,\beta\, e^{-.03R} + 0.2(1 - \beta)\left(e^{-0.258R} + 1.86\, e^{-1.63R}\right)\right) \quad (5.2\text{-}6)$$

where %T is the percent of time rain rate R is equalled or exceeded, M is the total accumulation in time T and β is the "thunderstorm factor." The measured value of M at VPI&SU is 620.8 mm over time T = 8088 hours. β was estimated from the curves published by Rice and Holmberg as 0.3. Using 5.2-6 the %T is plotted as a function of A_{eff} for elevation angles of 5, 30, 45 and 60 degrees in Figure 5.2-5 through 8. For low elevation angles both single and dual polarized systems have A_{eff} values greater than 30 dB for 0.01% of the time (52 minutes out of a year) and at 30 GHz the A_{eff} values are even higher. It is difficult to imagine a margin sufficient to overcome this much attenuation. For high reliability links, site diversity seems to be essential.

5.3 Link Availability Statistics

Whenever A_{eff} becomes greater than the system margin the link will not work or at best will work with degraded performance. For a synchronous communications satellite system the elevation angle α is fixed and the link availability can be calculated using equations 5.2-4 and 5.2-6. For the special case of the low orbit shuttle the percent of time a margin will be exceeded is a function of α. The margin calculated at $\alpha = 5°$ will be larger for α greater than 5° because of the smaller distance to the shuttle and the lower atmospheric losses. The percent of time an $\alpha = 5°$ margin of 10, 15

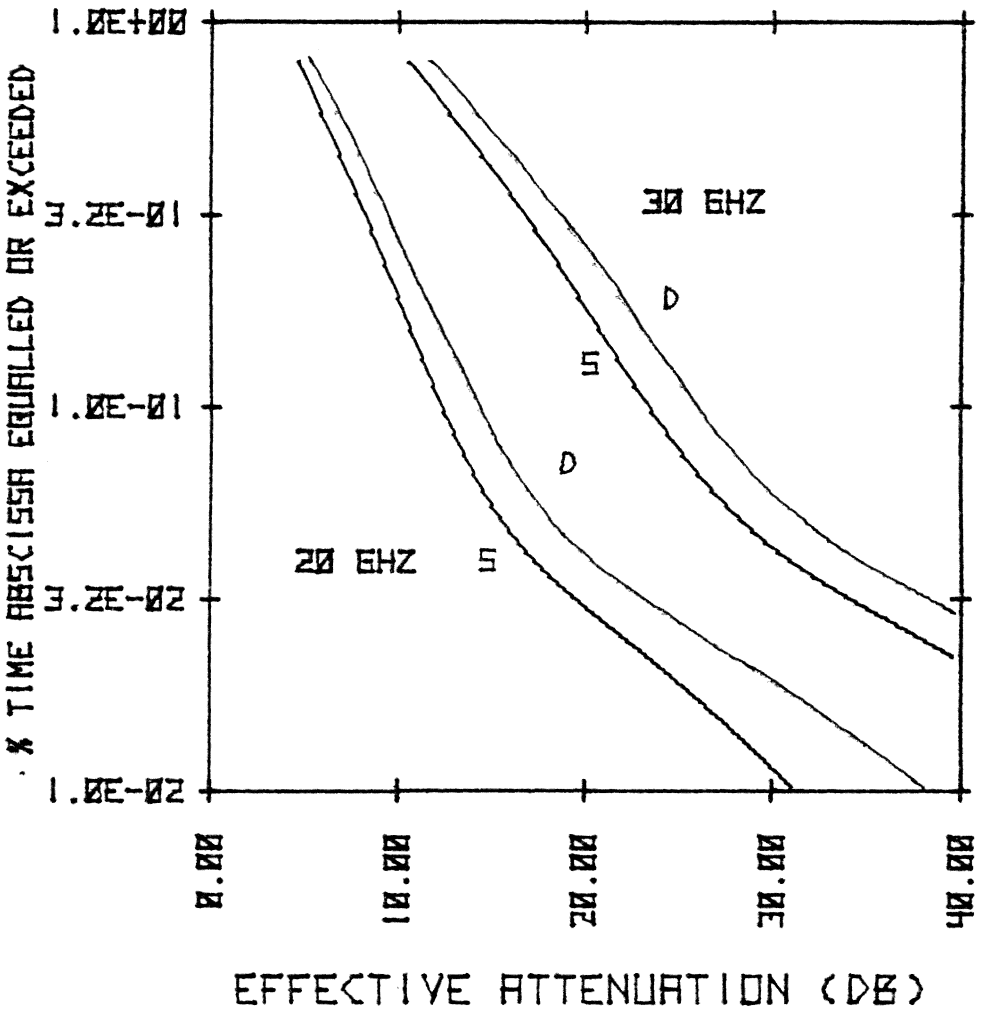

Figure 5.2-5. Percent of time a given A_{eff} is exceeded for dual (D) and single (S) polarized systems. Elevation angle is 5°.

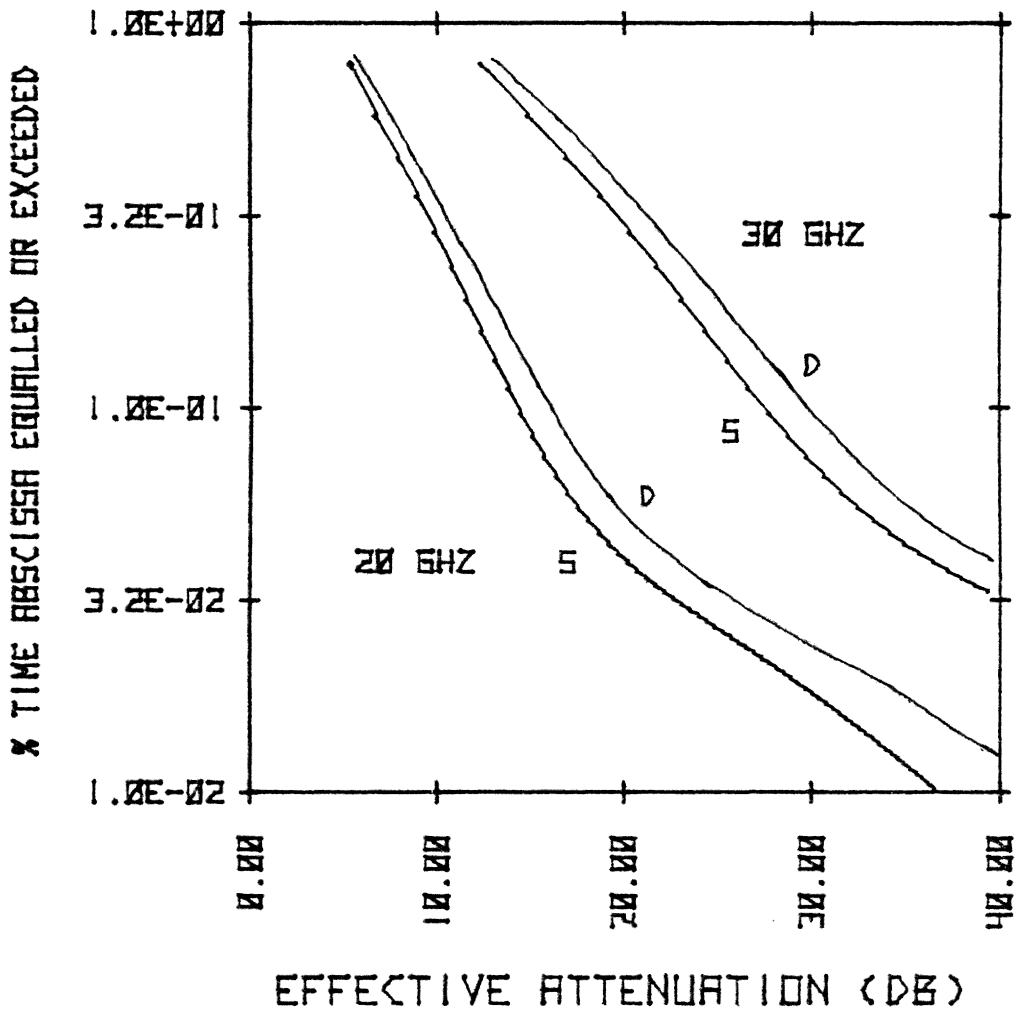

Figure 5.2-6. Percent of time a given A_{eff} is exceeded for dual (D) and single (S) polarized systems. Elevation angle is 30°.

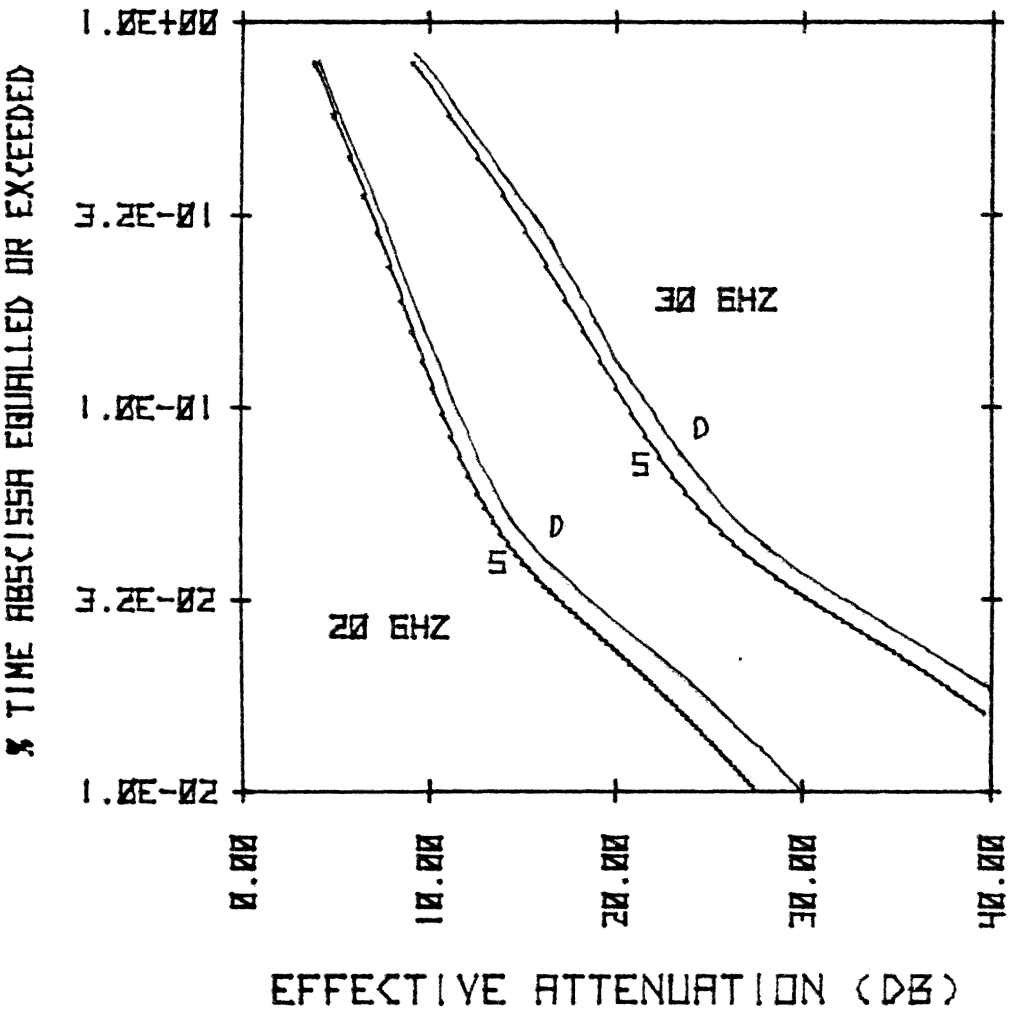

Figure 5.2-7. Percent of time a given A_{eff} is exceeded for dual (D) and single (S) polarized systems. Elevation angle is 45°.

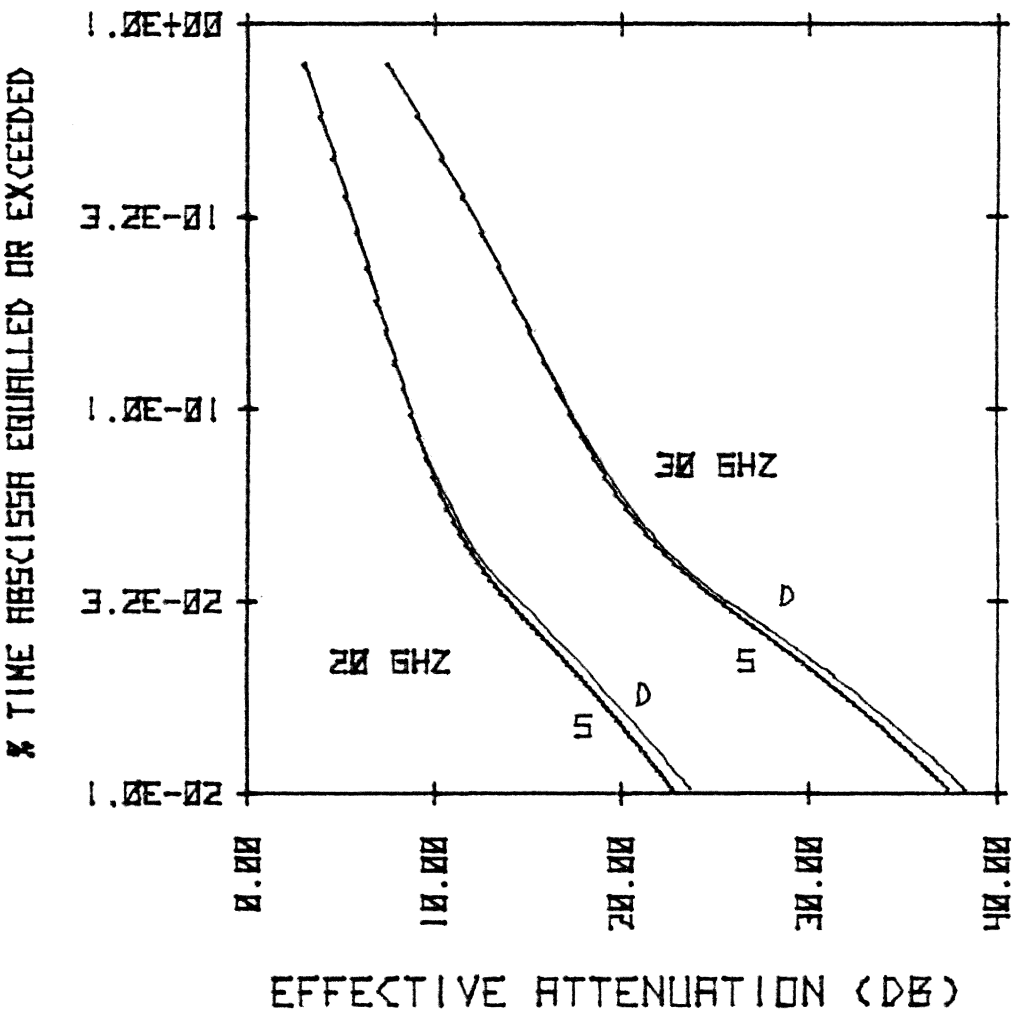

Figure 5.2-8. Percent of time a given A_{eff} is exceeded for dual (D) and single (S) polarized systems. Elevation angle is 60°.

and 20 dB will be exceeded is plotted in Figure 5.3-1 through 3. Once again the curves labelled D represent a dual polarized system and the curves labelled S represent a single polarized system. These curves were computed for the uplink only and the downlink only.

In the MWCE transponder mode rain will effect the uplink and downlink simultaneously and both will fade. Equations 5.1-1, 5.1-11 and the parameters listed in Table 5.1-1 were used to compute the curves in Figure 5.3-4. These curves show the percent of time the transponder will be unavailable as a function of elevation angle. Though the uplink margin is twice the downlink, the attenuation at 30 GHz is still the limiting factor on the link performance.

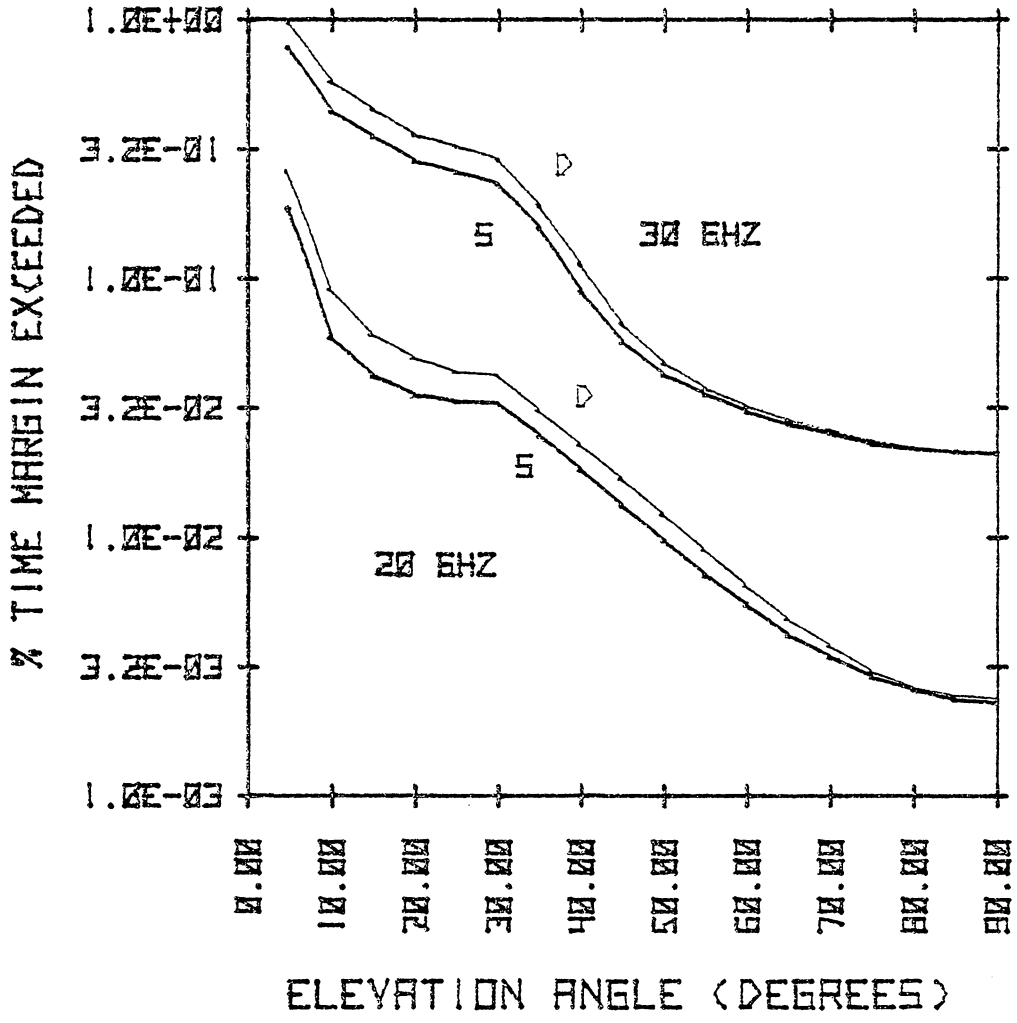

Figure 5.3-1. Percent of time a 10 dB at 5° elevation angle margin will be exceeded.

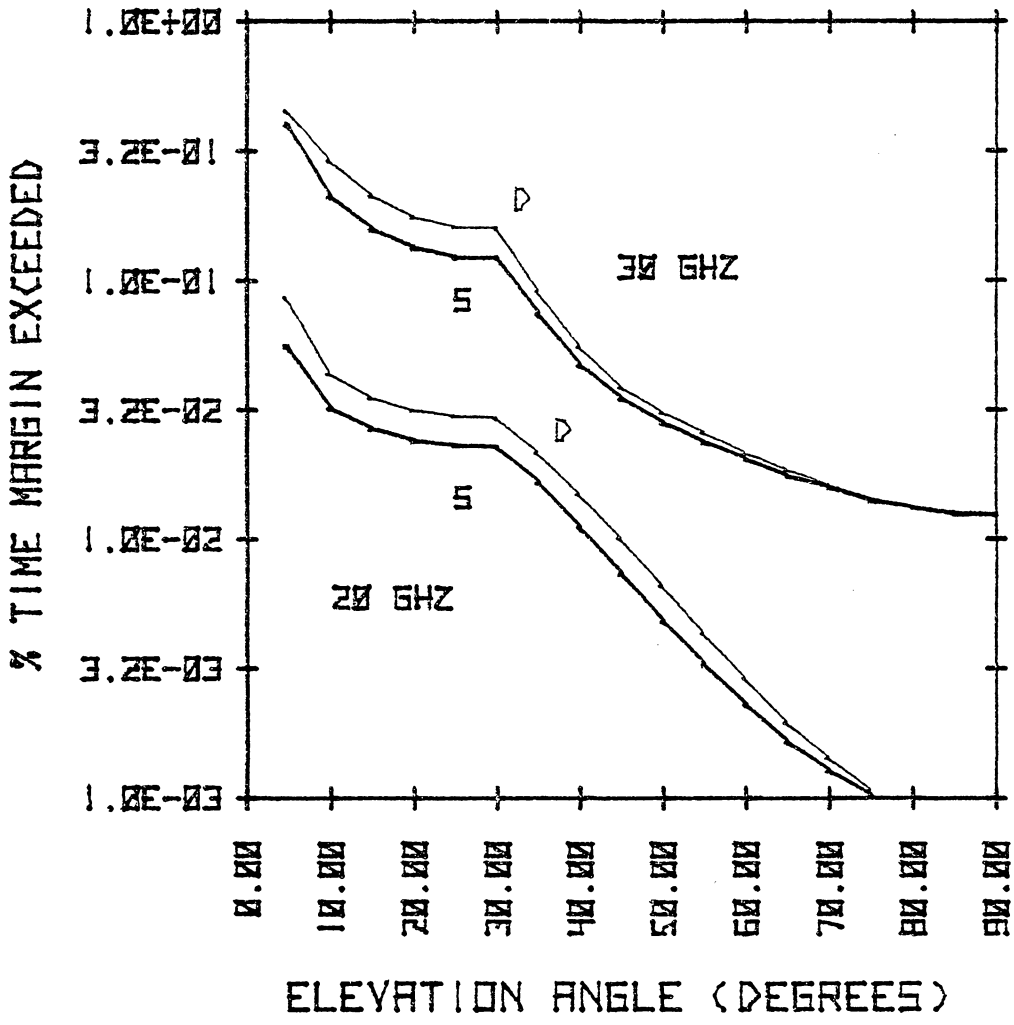

Figure 5.3-2. Percent of time a 15 dB at 5° elevation angle margin will be exceeded.

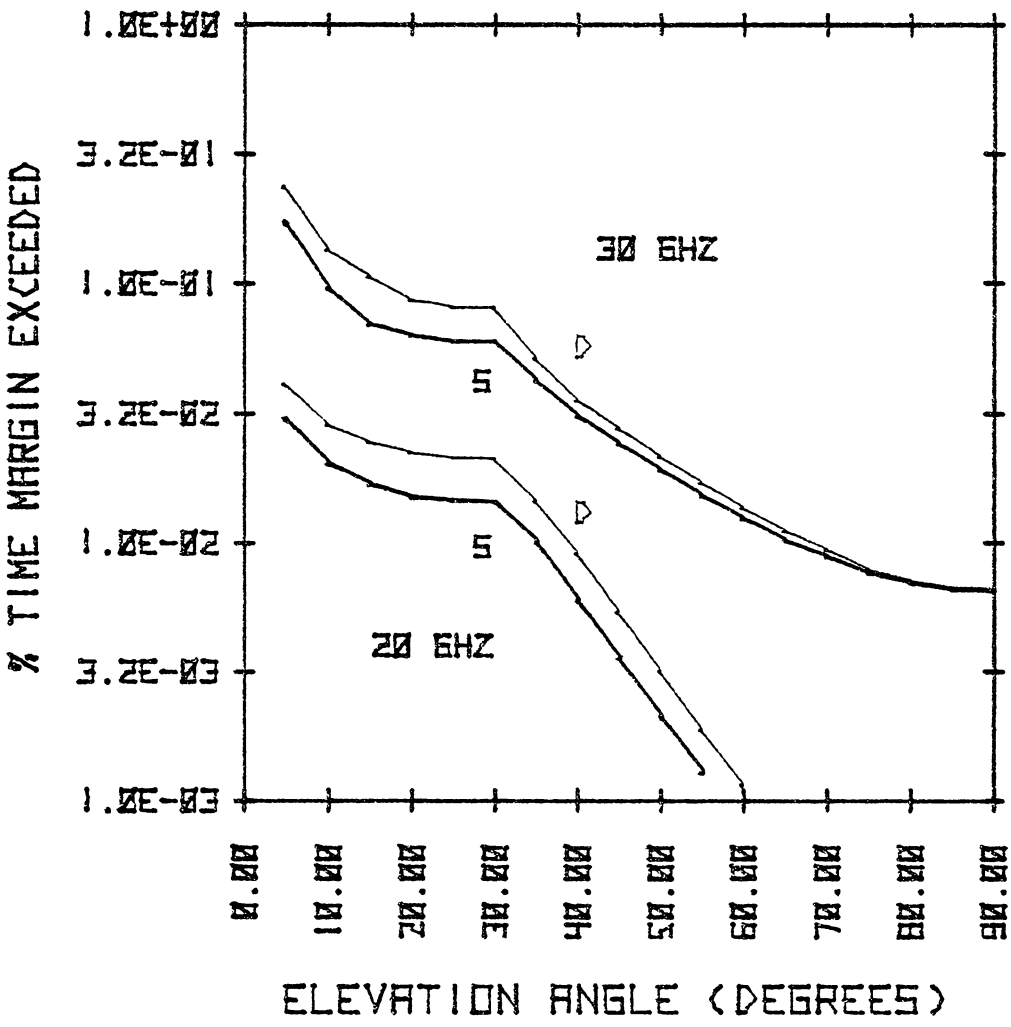

Figure 5.3-3. Percent of time a 20 dB at 5° elevation angle margin will be exceeded.

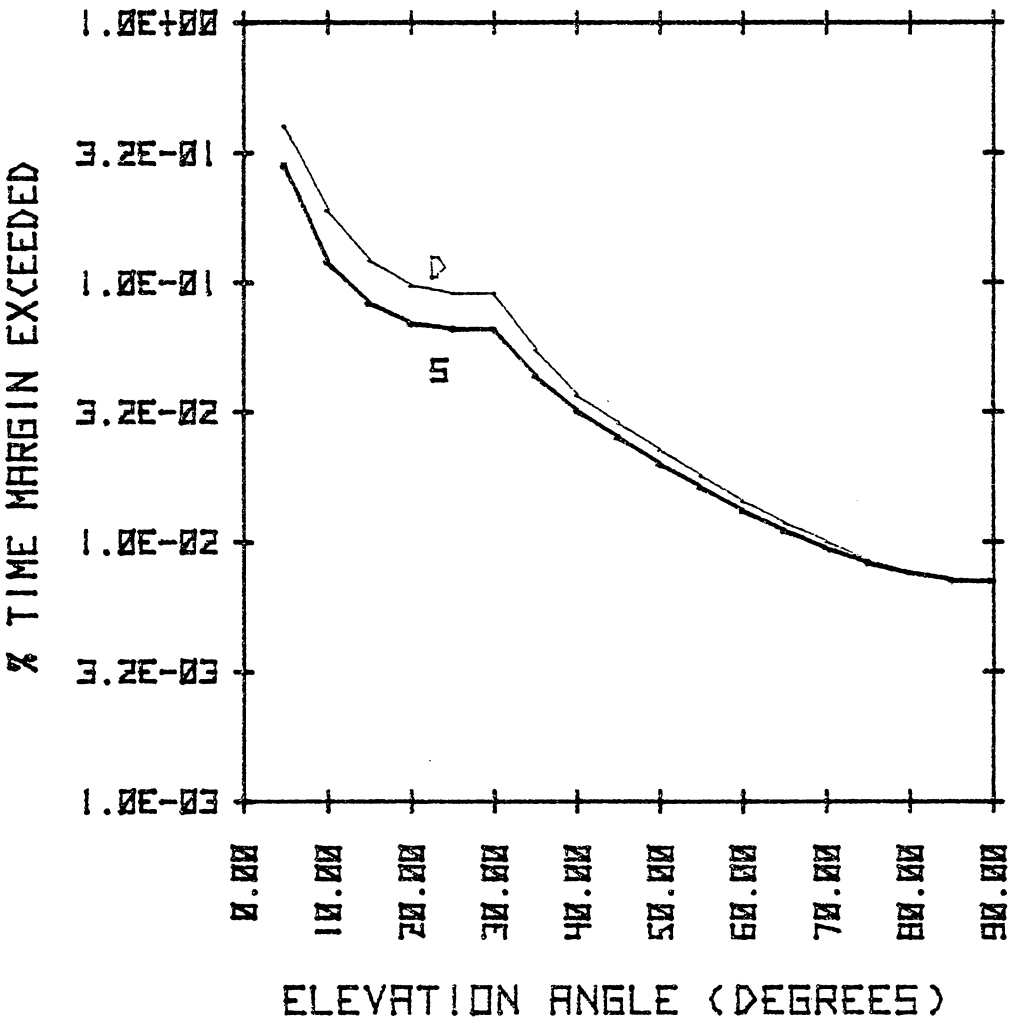

Figure 5.3-4. Percent of time a 10 dB margin at an elevation angle of 5° will be exceeded in the MWCE transponder mode.

CHAPTER 6

CONCLUSIONS

The requirements for a dual polarized 20 and 30 GHz digital satellite communications system have been presented and methods outlined for system calculations of rain effects. A *carrier to noise ratio degradation* has been defined which allows the effects of cross-talk between the dual polarized channels to be included in system power budgets.

A synthetic storm algorithm for computing rain attenuation has been discussed and compared to measured data. An *effective attenuation* has been defined which combines the effects of CNR degradation caused by depolarization (or any other crosstalk) and attenuation. It has been shown that the main impact of rain on 20 and 30 GHz communications is attenuation with depolarization being a secondary effect. A dual polarized system requires only one to three dB more margin to achieve the same outage time as a single polarized link. There are indications [33] that adaptive polarization systems can reduce this three dB difference significantly at small cost. However the outage times resulting from attenuation alone will be fairly large and site diversity seems the only available option if low outage times (less than .1% of the year) are required.

The specific case of the Millimeter Wave Communications Experiment (MWCE) was examined. This Spacelab payload will allow actual data transmission tests to be conducted on a dual polarized

20 and 30 GHz link. It will also make tests at very low elevation angles possible. Minimum MWCE ground station G/T and EIRP were calculated. Using the Rice and Holmberg rain rate model projections of attenuation and outage times for the VPI&SU location have been presented.

The use of an effective attenuation to combine the effects of rain depolarization and attenuation is a new development by the author and the synthetic storm algorithm was jointly developed by the author and R. R. Persinger. This thesis is the first time the various parameters affecting dual polarized satellite links at 20/30 GHz have been brought together in a form suitable for system calculations. Though calculations have been based on the parameters of the MWCE and the VPI&SU location, the methods presented can be applied to any digital 20 and 30 GHz space communications link, single or dual polarized.

REFERENCES

1. Horton, J. B., C. C. Allen, M. J. Massaro, J. L. Zemany, J. W. Murrell, R. W. Stanhouse, G. P. Condon, R. F. Stone, J. Swana, M. Afifi, R. Milton, "Feasibility and Systems Definition Study for Microwave Multi-Application Payload (MMAP)," NASA Contract NAS5-23734, General Electric Company, Valley Forge Space Center, P. O. Box 8555, Philadelphia, PA 19101

2. Whalen, A. D., *Detection of Signals in Noise*, Academic Press, New York, 1971, p. 75.

3. Prabhu, V. K., "Error Rate Considerations for Coherent PSK Systems with Co-channel Interference," *BSTJ*, March, 1969.

4. Rosenbaum, A. S., "PSK Error Performance with Gaussian Noise and Interference," *BSTJ*, February, 1968.

5. Juroshek, J. R., "Performance of Digital Modems with Co-channel Interference and Gaussian Noise," OT Report 76-82, U. S. Dept. of Commerce, Office of Telecommunications, Boulder, Colorado.

6. Juroshek, J. R., "An Approximate Method for Calculating the Performance of CPSK and NCFSK Modems in Gaussian Noise and Interference," OT-Report 77-109, U. S. Dept. of Commerce, Office of Telecommunications, Boulder, Colorado.

7. Crane, R. K., "Propagation Phenomena Affecting Satellite Communications Systems Operating in the Centimeter and Millimeter Wavelength Bands," *Proceedings of the IEEE*, Vol. 59, No. 2., February, 1971.

8. Hogg, D. C., "Millimeter-Wave Communication through the Atmosphere," *Science*, Vol. 159, No. 3810, p. 39-46, January 5, 1968.

9. Oguchi, T., "Attenuation of Electromagnetic Waves Due to Rain with Distorted Raindrops," *J. Radio Res. Lab.*, Jap., Vol. 7, 1960, pp. 467-485.

10. Morrison, J. A., and M. J. Cross, "Scattering of a Plane Electromagnetic Wave by Axisymmetric Raindrops," *Bell Syst. Tech. J.* 1974, 53 pp., 955-1019.

11. Uzunoglu, N. K., B. G. Evans, A. R. Holt, "Scattering of Electromagnetic Radiation by Precipitation Particles and Propagation Characteristics of Terrestrial and Space Communications Systems," *Proc. IEE*, Vol. 124, No. 5, May, 1977, pp. 417-242.

12. van de Hulst, H. C., *Light Scattering by Small Particles*, New York: John Wiley & Sons, Inc., 1957.

13. Thomas, D. T., "Cross Polarization Distortion in Microwave Radio Transmission due to Rain," *Radio Science*, Vol. 6, No. 10, Oct. 1971, pp. 833-840.

14. Laws, J. O., and D. A. Parsons, "The Relation of Raindrop-size to Intensity," *Trans. Am. Geophysical Union*, Vol. 24, 1943, pp. 432-460.

15. Watson, P. A., N. J. McEwan, S. I. Ghobrial, M. Arbabi, "Cross Polarisation Studies at 11 GHz," *Final Report*, European Space Research Organisation, Contract Number 1247/SL, U. of Bradford, Bradford, England, June 1973.

16. Chu, T. S., "Rain Induced Crosspolarisation of Centimetre and Millimetre Wavelengths," *Bell Syst. Tech. J.*, 1974, 53 pp. 1557-1579.

17. Jones, D. M. A., "The Shape of Raindrops," *Journal of Meteorology*, Vol. 16, October 1959, pp. 504-510.

18. Pruppacher, H. R. and R. L. Pitter, "A Semi-Empirical Determination of the Shape of Cloud and Raindrops," *J. Atmos. Sci.*, 1971, 28. pp. 86-94.

19. Wiley, P. H., C. W. Bostian, W. L. Stutzman, "The Influence of Polarization on Millimeter Wave Propagation Through Rain," *Interim Report I*, NASA Grant NGR-47-004-091, VPI&SU, Blacksburg, Virginia, June 1973.

20. Persinger, R. R., "Millimeter Wave Propagation Modeling of Inhomogeneous Rain Media for Satellite Communications Systems," M.S. Thesis, VPI&SU, May, 1978.

21. Saunders, M. J., "Crosspolarisation at 18 and 30 GHz due to Rain," *IEEE Trans.*, 1971, AP-19, pp. 273-277.

22. Brussaard, G., "A Meteorological Model for Rain-Induced Cross Polarization, *Trans. IEEE*, AP-24, 5-11, January, 1976.

23. Ippolito, L. J., "Correlation Measurements of 15.3 GHz Attenuation and Ground Rainfall Rate for an Earth-Satellite Path," *1972 G-AP International Symposium Programme and Digest*, December, 1972, pp. 256-259.

24. Hogg, D. C., T. S. Chu, "The Role of Rain in Satellite Communications," *Proceedings of the IEEE*, Vol. 63, No. 9, September, 1975, pp. 1308-1331.

25. Bostian, C. W., S. R. Kauffman, E. A. Manus, R. E. Marshall, W. P. Overstreet, R. R. Persinger, W. L. Stutzman, and P. H. Wiley, "Final Report: Second Year of Work, A Depolarization and Attenuation Experiment Using the COMSTAR and CTS Satellites," NASA Contract NAS5-22577, VPI&SU, Blacksburg, Virginia, February, 1978.

26. Hodge, D. B., "Frequency Scaling of Rain Attenuation," *IEEE Transactions on Antennas and Propagation*, Vol. AP-25, No. 3, pp. 446-447, May, 1977.

27. Harris, J. M., and G. Hyde, "Preliminary Results of COMSTAR 19/29-GHz Beacon Measurements at Clarksburg, Maryland," *Comsat Technical Review*, Vol. 7, No. 2, 1977, pp. 599-623.

28. Ippolito, L. J., "20- and 30-GHz Millimeter Wave Experiments with the ATS-6 Satellite," NASA TN D-8197, April 1976.

29. Rice, P. L., and N. R. Holmberg, "Cumulative Time Statistics of Surface-Point Rainfall Rates," *IEEE Transactions on Communications*, Vol. COM-21, No. 10, October, 1973, pp. 1131, 1136.

30. Watson, P. A., S. I. Ghobrial, "Off-Axis Polarization Characteristics of Cassegrain and Front Fed Paraboloidal Antennas," *IEEE Transactions on Antennas and Propagation*, Vol. AP-20, No. 6, November, 1972.

31. Stutzman, W. L., "A Depolarization and Attenuation Experiment Using the CTS and Comstar Satellite, Supplemental Report 1," NASA Contract NAS5-22577, VPI&SU, Blacksburg, VA, June, 1977.

32. Olsen, R. L., D. V. Rogers, D. B. Hodge, "The aR^b Relation in the Calculation of Rain Attenuation," *IEEE Transactions on Antenna and Propagation*, Vol. AP-26, No. 2, March, 1978.

33. Overstreet, W. P., "The Phase of the Crosspolarized Signal Generated by Millimeter Wave Propagation Through Rain," M.S. Thesis, VPI&SU, June, 1978.

APPENDIX

Distance from a ground station to an orbiting spacecraft as a function of ground station elevation angle. The geometry is shown in Figure A-1. From the law of sines

$$\frac{\sin(A)}{Re} = \frac{\sin(\alpha + \pi/2)}{Re + h_{sc}} = \frac{\cos(\alpha)}{Re + h_{sc}} \tag{A-1}$$

$$\sin(A) = \frac{Re}{Re + h_{sc}} \cos(\alpha)$$

$$A = \sin^{-1}\left[\frac{Re}{Re + h_{sc}} \cos(\alpha)\right] \tag{A-2}$$

Also from the law of sines

$$\frac{\sin(P)}{d_{sc}} = \frac{\cos(\alpha)}{Re + h_{sc}} \tag{A-3}$$

$$P = \pi - A - (\pi/2 + \alpha)$$

$$P = \pi/2 - A - \alpha$$

Substituting for P in (A-3) and rearranging yields

$$\sin(\pi/2 - A - \alpha) = \frac{d_{sc} \cos(\alpha)}{Re + h_{sc}}$$

$$\cos(A + \alpha) = \frac{d_{sc} \cos(\alpha)}{Re + h_{sc}} \quad . \tag{A-4}$$

Solving for d_{sc} yields

$$d_{sc} = \frac{\cos(A + \alpha)}{\cos(\alpha)} (Re + h_s) \quad . \tag{A-5}$$

Combining (A-2) and (A-5) yields

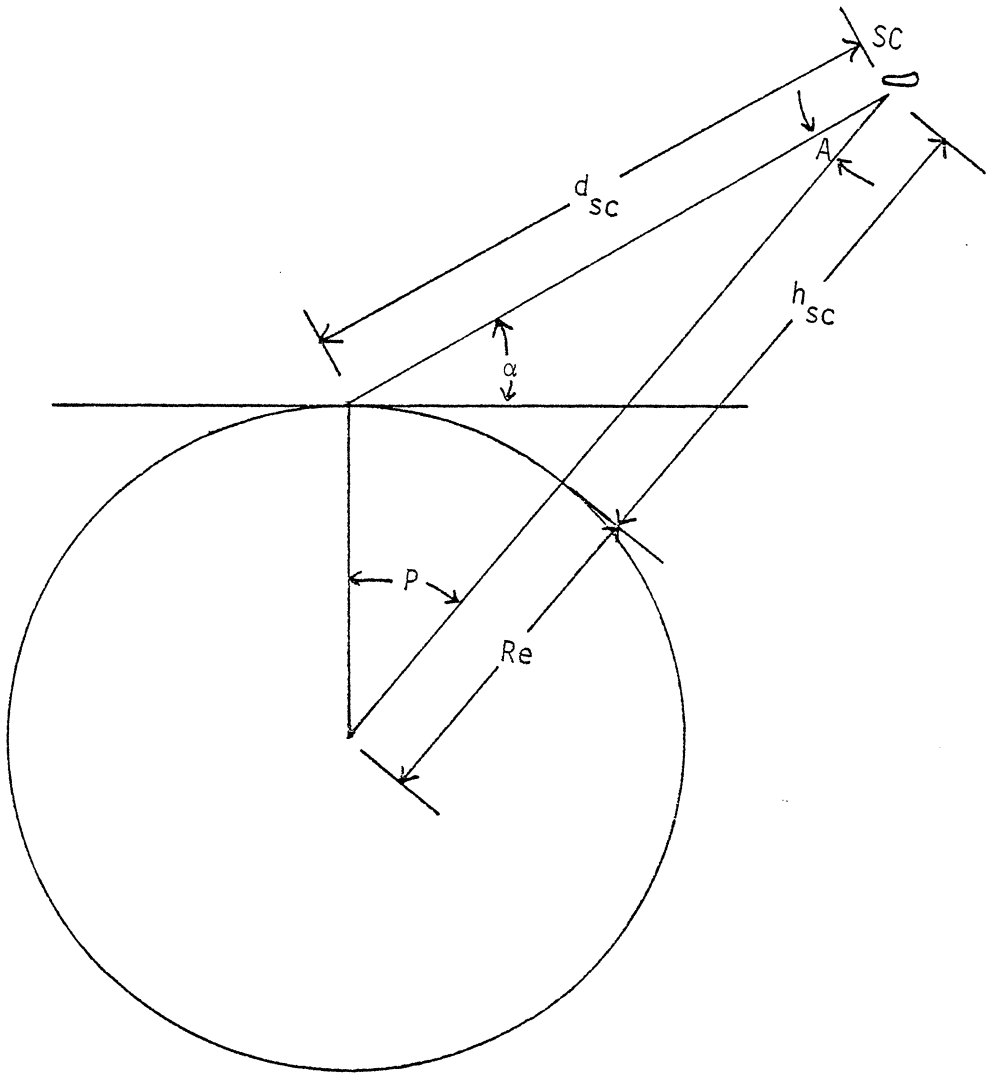

Figure A-1. Satellite orbit geometry.

$$d_{sc} = \cos\left[\sin^{-1}\left[\frac{Re}{Re + h_{sc}}\cos(\alpha)\right] + \alpha\right]\frac{Re + h_{sc}}{\cos(\alpha)} \quad . \qquad \text{(A-6)}$$

The vita has been removed from the scanned document

SYSTEM REQUIREMENTS FOR A DUAL POLARIZED
SPACE TO EARTH COMMUNICATIONS LINK

by

Robert Edward Castle, Jr.

(ABSTRACT)

System engineers are currently planning satellite communications links in the 20/30 GHz bands and frequency reuse through orthogonal polarizations. This thesis examines the system level constraints imposed by medium effects at these high frequencies of which the most serious is rain induced attenuation and depolarization.

The effect of crosstalk between orthogonal channels is calculated in terms of a degradation of the carrier to noise ratio. This concept is combined with the results of rain propagation modeling to define a rain induced *effective attenuation* which incorporates the effects of depolarization and attenuation. Methods for computing the effective attenuation and link outage times caused by rain are outlined which are applicable to any earth to space millimeter wave communication link. The Millimeter Wave Communications Experiment is used as an illustrative example of these methods.